Simultaneous Hand–Eye, Tool–Flange, and Robot–Robot Calibration for Comanipulation by Solving the $\mathbf{AXB = YCZ}$ Problem

Liao Wu, Jiaole Wang, *Student Member, IEEE*, Lin Qi, *Member, IEEE*, Keyu Wu, *Student Member, IEEE*, Hongliang Ren, *Member, IEEE*, and Max Q.-H. Meng, *Fellow, IEEE*

Abstract—Multirobot comanipulation shows great potential in surpassing the limitations of single-robot manipulation in complicated tasks such as robotic surgeries. However, a dynamic multirobot setup in unstructured environments poses great uncertainties in robot configurations. Therefore, the coordination relationships between the end-effectors and other devices, such as cameras (hand–eye calibration) and tools (tool–flange calibration), as well as the relationships among the base frames (robot–robot calibration) have to be determined timely to enable accurate robotic cooperation for the constantly changing configuration of the systems. We formulated the problem of hand–eye, tool–flange, and robot–robot calibration to a matrix equation $\mathbf{AXB = YCZ}$. A series of generic geometric properties and lemmas were presented, leading to the derivation of the final simultaneous algorithm. In addition to the accurate iterative solution, a closed-form solution was also introduced based on quaternions to give an initial value. To show the feasibility and superiority of the simultaneous method, two nonsimultaneous methods were compared through thorough simulations under various robot movements and noise levels. Comprehensive experiments on real robots were also performed to further validate the proposed methods. The comparison results from both simulations and experiments demonstrated the superior accuracy and efficiency of the proposed simultaneous calibration method.

Index Terms—$\mathbf{AXB = YCZ}$, calibration, cooperative manipulators, hand–eye calibration, identification.

NOMENCLATURE

$\mathbf{A}$	Homogeneous transformation matrix from base frame of sensor robot to its hand frame.
$\mathbf{B}$	Homogeneous transformation matrix from eye frame of sensor robot to tool frame of marker robot.
$\mathbf{C}$	Homogeneous transformation matrix from base frame of marker robot to its flange frame.
e	Error between calibration results and true values.
$\mathbf{E}$	Error matrix representing the inconsistency between calculated solutions and experiment data.
$\mathbf{F}$	Jacobian matrix for the iterative solution to rotational components.
$\mathbf{J}$	Coefficient matrix for the solution to translational components.
$\mathbf{K}$	Submatrix of the Jacobian matrix for solvability analysis.
$\mathbf{q}$	Quaternion.
$\mathbf{R}$	Rotation matrix.
$\mathbf{r}$	Vector representing elements of Lie algebra corresponding to a rotation.
$\mathbf{t}$	Translation vector.
$\mathbf{v}$	Eigenvector of matrix $\mathbf{W}^T \mathbf{W}$ for the closed-form solution to rotational components.
$\mathbf{W}$	Coefficient matrix for the closed-form solution to rotational components.
$\mathbf{X}$	Homogeneous transformation matrix from hand frame of sensor robot to its eye frame.
$\mathbf{Y}$	Homogeneous transformation matrix from base frame of sensor robot to base frame of marker robot.
$\mathbf{Z}$	Homogeneous transformation matrix from flange frame of marker robot to its tool frame.
Axis($\bullet$)	Unit axis of a rotation matrix.
Diag($\bullet$)	Diagonal matrix whose diagonal elements are listed in the brackets.
Exp($\bullet$)	Exponential map of a Lie algebra.
$LQ(\bullet)$	Multiplication matrix form of a quaternion which is left-multiplied to another quaternion.
$RQ(\bullet)$	Multiplication matrix form of a quaternion which is right-multiplied to another quaternion.
Rank($\bullet$)	Rank of a matrix.
Rot($\bullet, \bullet$)	Rotation about an axis for a certain angle.

L. Wu was with the Department of Biomedical Engineering, National University of Singapore, Singapore 119077. He is now with the School of Electrical Engineering and Computer Science, Queensland University of Technology, Brisbane, QLD 4000, Australia (e-mail: liao.wu@qut.edu.au).

J. Wang is with the Department of Electronic Engineering, The Chinese University of Hong Kong, Hong Kong (e-mail: jlwang@ee.cuhk.edu.hk).

L. Qi is with the Sino-Dutch Biomedical and Information Engineering School, Northeastern University, Shenyang 110819, China (e-mail: qilin@bmie.neu.edu.cn).

K. Wu and H. Ren are with the Department of Biomedical Engineering, National University of Singapore, Singapore 119077 (e-mail: keyu_wu@u.nus.edu; ren@nus.edu.sg).

M. Q.-H. Meng is with the Department of Electronic Engineering, The Chinese University of Hong Kong, Hong Kong, and affiliated with the State Key Laboratory of Robotics and Systems at Harbin Institute of Technology, China (e-mail: max@ee.cuhk.edu.hk).

$\theta(\bullet)$	Angle of a rotation matrix.
$[\bullet]^{\wedge}$	Skew-symmetric matrix of a vector.
$\bullet \circ \bullet$	Product of two quaternions.
$(\bullet)_i$	The ith column of a matrix.
$\|\bullet\|$	Norm of a vector or a matrix.
$|\bullet|$	Determinant of a square matrix.

I. INTRODUCTION

MULTIROBOT comanipulation provides a method for accomplishing tasks that are too complicated or even impossible for a single robot [1]. Many cooperative multirobot systems have been employed in the applications of robotic surgery [2]–[6], space and underwater exploration [7], payload transportation [1], [8], among others.

In the case of robotic surgery, multirobot comanipulation opens new possibilities for minimally invasive procedures. Despite state-of-the-art minimally invasive robotic systems, such as the da Vinci Surgical System (Intuitive Surgical Inc.) [9] and NOTES systems [10], which are capable of providing higher precision, less invasion, minimal pain, and blood loss, etc., compared with the traditional surgical paradigm, the procedures are still challenging, with constrained visualization and manipulation by the small entry incisions. Instead of building one bulky and complex robotic system, Lehman *et al.* [2] proposed to use many simple robotic systems to carry out the surgical procedure cooperatively. Their study has shown the plausibility of multirobot systems in surgical applications.

In previous studies on multirobot systems, the main focuses included collision avoidance and path planning [11], [12], mapping and navigation [13], object tracking [14], etc. However, less attention has been paid to the multirobot calibration problem, even though it is a vital part for multirobot comanipulation. In view of the importance of multirobot comanipulation in various applications, we focus on the fundamental calibration problem in this study. Special attention has been devoted to the paired-robot calibration for comanipulation, which is considered as the cornerstone of many multirobot scenarios.

Generally, multirobot comanipulation systems can be classified into either static or dynamic setups in terms of base mobility and manipulation variability. In the static setup, all bases of the involved robots are immobile, manipulation tasks remain unvaried so that tools do not need to be frequently changed, and the multiple robotic systems interact in a relatively simple way. In this case, the relationships among each base frame (robot–robot calibration) can be coarsely estimated from the mechanical design. In addition, the relationships between the end-effectors and other devices, such as cameras (hand–eye calibration) and tools (tool–flange calibration), can be estimated from traditional calibration methods. Nevertheless, independent estimations for all the unknowns will cause inaccuracy and inconsistency in a global sense for the whole system.

The dynamic setup is subjected to uncertainties due to base mobility of the member robots, variety of tasks, and changing environments. Uncertainties in the dynamically changing configuration of the robotic system make it impossible to perform cooperatively among the member mobile robots in the absence of the robot-to-robot relationships. Uncertainties in the varying environment burden the robots' ability to change tools and/or sensors in order to deal with different situations. Consequently, the hand–eye, tool–flange, and robot–robot relationships have to be determined in order to enable the robots to cooperate inside a changing environment.

A. Related Work

Hand–eye calibration [15]–[17] has been a classical problem when using a wrist-mounted sensor (such as a camera, a range-finder, etc.) to carry out various tasks. As shown in Fig. 1(a), the calibration problem can be formulated by a matrix equation as $\mathbf{AX} = \mathbf{XB}$, where $\mathbf{A}$ and $\mathbf{B}$ are the homogeneous transformation matrices of the end-effector and the camera between two relative robot movements, and $\mathbf{X}$ is the unknown relationship between the robot wrist and the sensor. This equation is solvable, provided that there are at least two motions with nonparallel rotation axes [18]. The hand–eye calibration problem has been thoroughly studied by many researchers, and ample methods have been proposed [19]–[24].

Extended from the hand–eye calibration, the simultaneous tool–flange and robot–world calibration, as shown in Fig. 1(b), defines a problem in which the relationship between the world frame and robot base frame is unknown in addition to the unknown relationship between the last joint of the robot and the rigidly mounted sensor/marker [25]–[27]. This new problem can be expressed as a homogeneous transformation equation $\mathbf{AX} = \mathbf{YB}$, where $\mathbf{Y}$ is the robot-to-world rigid transformation. Similarly, this simultaneous tool–flange and robot–world calibration problem can be solved by moving the robot twice with respect to two nonparallel rotational axes [25], and it has been well studied in [28]–[30]. It is noted that the aforementioned two calibration problems usually involve a static setup whereby the robot bases are immobile.

Robot–robot calibration emerges from the recent development of unmanned aerial vehicle [31]. In order to carry out tasks cooperatively, the relative robot-to-robot translation and rotation must be known beforehand, which results in this robot–robot calibration problem. Zhou and Roumeliotis [32] summarized that by considering all possible combinations of interrobot measurements, the robot-to-robot homogeneous transformation has a minimum of 14 base situations. The closed-form and analytic solutions have been given except for two singular situations. However, the previous work has been limited in the scope of cooperative measuring and sensing, which requires further study for the practice of comanipulation.

B. Proposed Method and Original Contributions

In this paper, we propose a novel method to solve the hand–eye, tool–flange, and robot–robot calibration problem for robotic comanipulation simultaneously. Distinguished from the previous approaches, the method formulates the problem as solving an $\mathbf{AXB} = \mathbf{YCZ}$ problem. Compared with two other nonsimultaneous methods based on the $\mathbf{AX} = \mathbf{XB}$ or $\mathbf{AX} = \mathbf{YB}$ equations, the proposed simultaneous method reduces both the difficulty in data acquisition and the inaccuracy caused by error propagation and accumulation.
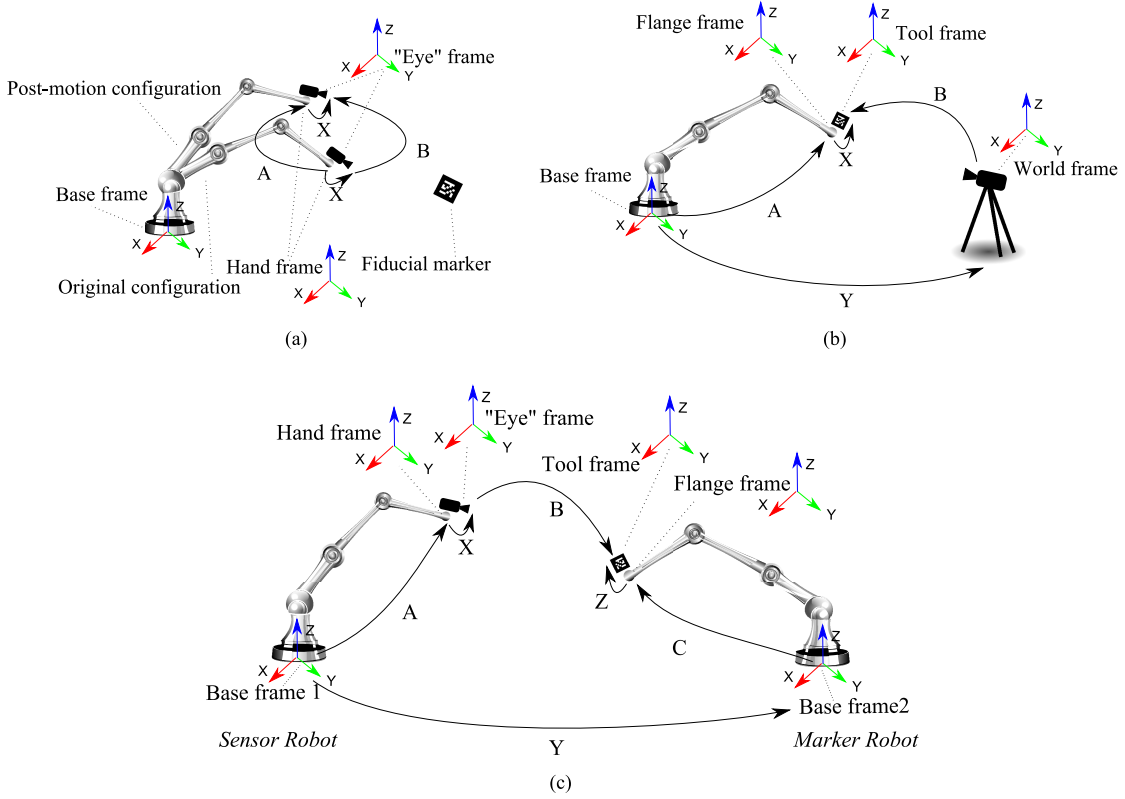
Fig. 1. Relevance and differences among the problem defined in this paper and two other classical calibration problems. Our problem formulation (c) can be considered as a superset of the two other problems (a) and (b). (a) Hand–eye calibration that can be formulated as an $\mathbf{AX} = \mathbf{XB}$ problem. (b) Robot–world and tool–flange calibration problem that can be formulated to an $\mathbf{AX} = \mathbf{YB}$ matrix equation. (c) Hand–eye, tool–flange, and robot–robot calibration problem that can be formulated in a matrix equation as $\mathbf{AXB} = \mathbf{YCZ}$.

This paper is an improved version of our previous work [33] in which a formulation of the calibration of multiple robot comanipulation was introduced and an iterative method was proposed. In this paper, the extended contributions include the following:

1) a closed-form solution that provides an initial point for the further iteratively refined solution, making the method more complete;
2) a thorough mathematical interpretation, solvability analysis, and related proofs;
3) real-robot experiments that demonstrate the effectiveness of the proposed methods.

The rest of the paper is organized as follows: Section II models and formulates the calibration problem, followed by the proposed solutions, mathematical interpretations and algorithms, and solvability analysis. The simulation results of the algorithm comparison are illustrated in Section III. Section IV describes the experiments carried out to evaluate the proposed methods. We further discuss the results and the gained insights in Section V and draw some conclusions at the end of this paper.

II. METHODS

A. Problem Formulation

The scenario for the hand–eye, tool–flange, and robot–robot calibration addressed in this paper is illustrated in Fig. 1(c) in which two robots, one grasping a sensor and the other grasping a marker, are both located inside of a sensing scope.

The homogeneous transformations of the hand and flange frames with respect to the robot base frames are denoted as the measurable data $\mathbf{A}_i$ and $\mathbf{C}_i$, respectively. The homogeneous transformation of the tool held by one robot hand with respect to the sensor ("eye") held by the other is denoted as $\mathbf{B}_i$, which is also measurable using a sensor (such as optical tracker, camera, etc.) and a marker (such as LED, reflecting ball, fiducial pattern, etc.). In both cases, the i stands for the ith measurement. An assumption made here is that the forward kinematics of the robots is derivable, which is reasonable since the structure parameters are often provided by the manufacturers. Currently, most commercial robots have repeatability precision at submillimeters. If the robot suffers from low position accuracy, ample calibration methods are available to calibrate the robot kinematics [34], [35].

The three unknowns are defined as the homogeneous transformations from one robot base frame to another ($\mathbf{Y}$), and from eye/tool to robot hand/flange ($\mathbf{X}$ and $\mathbf{Z}$), respectively. The aforementioned measurable data $\mathbf{A}$, $\mathbf{B}$, and $\mathbf{C}$ and the unknowns $\mathbf{X}$, $\mathbf{Y}$, and $\mathbf{Z}$ form a transformation loop, which can be formulated as

$$\mathbf{AXB} = \mathbf{YCZ}. \tag{1}$$

B. Solutions

1) Three-Step Method: In the nonsimultaneous three-step method, the $\mathbf{X}$ and $\mathbf{Z}$ in (1) are separately calculated in the first

two steps as two hand-eye/tool-flange calibrations represented by an $\mathbf{AX} = \mathbf{XB}$ problem. This requires two data acquisition procedures in which the two manipulators individually carry out at least two rotations about nonparallel axes. The last unknown robot–robot relationship $\mathbf{Y}$ can then be solved directly by using the previously retrieved data by the method of least squares.

2) Two-Step Method: The nonsimultaneous two-step method resolves the original calibration problem in successive processes by first solving the $\mathbf{AX} = \mathbf{XB}$ equation and then the $\mathbf{AX} = \mathbf{YB}$ equation. The data acquisition procedures and obtained data are the same as the three-step method. In contrast with solving robot–robot relationship independently, the two-step method solves both tool–flange/hand–eye and robot–robot transformations in the second step's $\mathbf{AX} = \mathbf{YB}$ manner. This is possible because equation $\mathbf{AXB} = \mathbf{YCZ}$ can be expressed as $(\mathbf{AXB})\mathbf{Z}^{-1} = \mathbf{YC}$, which is in an $\mathbf{AX} = \mathbf{YB}$ form, where $\mathbf{A}$, $\mathbf{B}$, $\mathbf{X}$, and $\mathbf{Y}$ correspond to $\mathbf{AXB}$, $\mathbf{C}$, $\mathbf{Z}^{-1}$, and $\mathbf{Y}$ in the original equation, respectively.

3) Proposed Simultaneous Method: Since the three-step and two-step methods use previous solutions as inputs in latter steps, they both face a problem of error accumulation. In addition to accuracy errors, the efficiency of these two methods is also improvable. Rather than keeping one robot static while calibrating the other robot, it is more time and work efficient to have the two robots participate in the calibration procedure simultaneously.

In regard to this, a simultaneous method is proposed to improve the accuracy and efficiency of the calibration by solving the original $\mathbf{AXB} = \mathbf{YCZ}$ problem directly. During the data acquisition procedure, the manipulators simultaneously change to different configuration, and the corresponding dataset $\mathbf{A}$, $\mathbf{B}$, and $\mathbf{C}$ are recorded. Then, the unknown $\mathbf{X}$, $\mathbf{Y}$, and $\mathbf{Z}$ are solved simultaneously. The detailed algorithm and mathematical interpretations are introduced in Sections II-C and II-D.

C. Algorithm Development

In this part, the algorithm of the aforementioned simultaneous calibration method is introduced. In the algorithm, the rotational and translational components are separately solved for the three unknowns in the $\mathbf{AXB} = \mathbf{YCZ}$ equation. By expanding the homogeneous transformation matrices, the following two equations can be derived:

$$\mathbf{R}_A \mathbf{R}_X \mathbf{R}_B = \mathbf{R}_Y \mathbf{R}_C \mathbf{R}_Z \qquad (2)$$

$$\mathbf{R}_A \mathbf{R}_X \mathbf{t}_B + \mathbf{R}_A \mathbf{t}_X + \mathbf{t}_A = \mathbf{R}_Y \mathbf{R}_C \mathbf{t}_Z + \mathbf{R}_Y \mathbf{t}_C + \mathbf{t}_Y \quad (3)$$

where $\mathbf{R}$ is a 3×3 rotation matrix, and $\mathbf{t}$ is a 3×1 translation vector. We will first solve $\mathbf{R}_X$, $\mathbf{R}_Y$, $\mathbf{R}_Z$ from (2) and then find $\mathbf{t}_X$, $\mathbf{t}_Y$, $\mathbf{t}_Z$ from (3) by using the solved rotation matrices.

1) Closed-Form Solution to the Rotational Components: The rotational components can be solved in a closed-form manner based on quaternions.

According to the relationship between quaternions and rotation matrices, we can obtain the following equation from (2):

$$\mathbf{q}_A \circ \mathbf{q}_X \circ \mathbf{q}_B = \mathbf{q}_Y \circ \mathbf{q}_C \circ \mathbf{q}_Z \qquad (4)$$

where $\mathbf{q}_i = [q_{i0} \ q_{i1} \ q_{i2} \ q_{i3}]^T (i = A, B, C, X, Y, Z)$ is the unit quaternion associated with $\mathbf{R}_i$, and operator $\circ$ represents the

quaternion multiplication. Based on the algebra of quaternions, (4) can be written in matrix forms as

$$RQ(\mathbf{q}_B)LQ(\mathbf{q}_A)\mathbf{q}_X = RQ(\mathbf{q}_Z)LQ(\mathbf{q}_Y)\mathbf{q}_C. \qquad (5)$$

According to [26], $RQ(\mathbf{q})$ and $LQ(\mathbf{q})$ in (5) are defined as

$$RQ(\mathbf{q}) = \begin{bmatrix} q_0 & -q_1 & -q_2 & -q_3 \\ q_1 & q_0 & q_3 & -q_2 \\ q_2 & -q_3 & q_0 & q_1 \\ q_3 & q_2 & -q_1 & q_0 \end{bmatrix} \qquad (6)$$

$$LQ(\mathbf{q}) = \begin{bmatrix} q_0 & -q_1 & -q_2 & -q_3 \\ q_1 & q_0 & -q_3 & q_2 \\ q_2 & q_3 & q_0 & -q_1 \\ q_3 & -q_2 & q_1 & q_0 \end{bmatrix}. \qquad (7)$$

Observing (5), we can find that there is a strong coupling between $\mathbf{q}_Y$ and $\mathbf{q}_Z$. Therefore, it is difficult to solve these two unknowns directly. To avoid dealing with complex nonlinear equations, we define an intermediate variable

$$\mathbf{q}_{YZ} =$$

$$\begin{bmatrix} q_{Y0}q_{Z0} & q_{Y0}q_{Z1} & q_{Y0}q_{Z2} & q_{Y0}q_{Z3} & q_{Y1}q_{Z0} & q_{Y1}q_{Z1} \end{bmatrix}$$

$$\begin{matrix} q_{Y1}q_{Z2} & q_{Y1}q_{Z3} & q_{Y2}q_{Z0} & q_{Y2}q_{Z1} & q_{Y2}q_{Z2} & q_{Y2}q_{Z3} \end{matrix}$$

$$q_{Y3}q_{Z0} \quad q_{Y3}q_{Z1} \quad q_{Y3}q_{Z2} \quad q_{Y3}q_{Z3} \big]^T \big|_{16 \times 1}. \qquad (8)$$

Here (and hereinafter), the subscript after a vertical bar indicates the size of a vector or matrix after transposition. Then, the right side of (5) can be written as

$$RQ(\mathbf{q}_Z)LQ(\mathbf{q}_Y)\mathbf{q}_C = \mathbf{W}_C \mathbf{q}_{YZ} \qquad (9)$$

where $\mathbf{W}_C$ is a 4×16 matrix constructed by the elements of $\mathbf{q}_C$.

Meanwhile, the left side of (5) can also be denoted as $\mathbf{W}_{AB}\mathbf{q}_X$, where $\mathbf{W}_{AB} = RQ(\mathbf{q}_B)LQ(\mathbf{q}_A)$.

Now, we can define

$$\mathbf{W}_{ABC} = [\mathbf{W}_{AB} \ -\mathbf{W}_C]_{4 \times 20} \qquad (10)$$

$$\mathbf{q}_{XYZ} = [\mathbf{q}_X^T \ \mathbf{q}_{YZ}^T]^T \big|_{20 \times 1} \qquad (11)$$

and (5) is equivalent to

$$\mathbf{W}_{ABC}\mathbf{q}_{XYZ} = \mathbf{0}. \qquad (12)$$

If m different independent measurements are provided, we can combine these equations together as

$$\tilde{\mathbf{W}}_{ABC}\mathbf{q}_{XYZ} = \mathbf{0} \qquad (13)$$

where

$$\tilde{\mathbf{W}}_{ABC} = \begin{bmatrix} \mathbf{W}_{ABC,1}^T \ \mathbf{W}_{ABC,2}^T \ \cdots \ \mathbf{W}_{ABC,m}^T \end{bmatrix}^T \big|_{4m \times 20} \qquad (14)$$

and then solving $\mathbf{q}_{XYZ}$ is equivalent to finding the vector that minimizes the cost function

$$f(\mathbf{q}_{XYZ}) = \mathbf{q}_{XYZ}^T \tilde{\mathbf{W}}_{ABC}^T \tilde{\mathbf{W}}_{ABC}\mathbf{q}_{XYZ}. \qquad (15)$$

According to the min–max theorem [36] and the fact that the norm of $\mathbf{q}_{XYZ}$ is constant ($\|\mathbf{q}_{XYZ}\| = \sqrt{2}$), the solution $\mathbf{q}_{XYZ}$ that minimizes (15) is parallel to the eigenvector $\mathbf{v}_{XYZ}$

of $\tilde{\mathbf{W}}_{ABC}^T \tilde{\mathbf{W}}_{ABC}$ associated with the minimum eigenvalue. When $\mathbf{v}_{XYZ}$ is found, the rest is quite straightforward. Suppose $\mathbf{v}_{XYZ}$ is denoted in the same way as (11), i.e.,

$$\mathbf{v}_{XYZ} = [\mathbf{v}_X^T \ \mathbf{v}_{YZ}^T]^T \big|_{20 \times 1} \tag{16}$$

then

$$\mathbf{q}_X = \mathbf{v}_X / \|\mathbf{v}_X\| \tag{17}$$

$$\mathbf{q}_{YZ} = \mathbf{v}_{YZ} / \|\mathbf{v}_{YZ}\|. \tag{18}$$

The elements of $\mathbf{q}_Y$ and $\mathbf{q}_Z$ can be calculated based on the elements of $\mathbf{q}_{YZ}$. $\mathbf{R}_X$, $\mathbf{R}_Y$, and $\mathbf{R}_Z$ can then be converted from $\mathbf{q}_X$, $\mathbf{q}_Y$, and $\mathbf{q}_Z$, respectively.

It is important to note that the algorithm discussed above does not consider the ambiguity of the mapping from rotation matrices to quaternions. Actually, a quaternion multiplying itself by -1 corresponds to the same rotation matrix. As a result, in some cases, (4) should be expressed as

$$\mathbf{q}_A \circ \mathbf{q}_X \circ \mathbf{q}_B = -\mathbf{q}_Y \circ \mathbf{q}_C \circ \mathbf{q}_Z \tag{19}$$

and (10) as

$$\mathbf{W}_{ABC} = [\mathbf{W}_{AB} \ \mathbf{W}_C]_{4 \times 20}. \tag{20}$$

This leads to troubles in practical implementation of the algorithm, as we do not know whether to use (10) or (20) to formulate the algorithm in advance. (A more detailed explanation can be found in Appendix A.) A feasible solution is to enumerate all the possibilities and choose the case in which the minimal eigenvalue of $\tilde{\mathbf{W}}_{ABC}^T \tilde{\mathbf{W}}_{ABC}$ is closest to zero. However, this works only for situations in which the measurement number m is small because the calculation cost increases exponentially with m. In addition, since the above algorithm simply treats the nonlinearly constrained problem as an unconstrained one, the accuracy of the solution is affected. Hence, this method is more suitable for generating an approximate initial solution, and only a small portion of the large amount of measurement data is required, saving much computational cost. An iterative refining algorithm that gives a more accurate solution will be introduced in the next section.

2) Iterative Solution to the Rotational Components: Since a rotation matrix belongs to the Lie group $SO(3)$, it can be exponentially mapped by its Lie algebra $[\mathbf{r}]^\wedge$ [37], that is,

$$\mathbf{R} = Exp\left([\mathbf{r}]^\wedge\right) = \mathbf{I} + \frac{\sin(\|\mathbf{r}\|)}{\|\mathbf{r}\|}[\mathbf{r}]^\wedge + \frac{1 - \cos(\|\mathbf{r}\|)}{\|\mathbf{r}\|^2}\left([\mathbf{r}]^\wedge\right)^2 \tag{21}$$

where $\|\mathbf{r}\|$ gives the norm of the vector $\mathbf{r} = [r_1 \ r_2 \ r_3]^T$, and $[\mathbf{r}]^\wedge$ is the skew-symmetric matrix of $\mathbf{r}$ that is given by

$$[\mathbf{r}]^\wedge = \begin{bmatrix} 0 & -r_3 & r_2 \\ r_3 & 0 & -r_1 \\ -r_2 & r_1 & 0 \end{bmatrix}. \tag{22}$$

Using the Taylor series expansion of the exponential map, we have

$$\mathbf{R} = Exp\left([\mathbf{r}]^\wedge\right) = \mathbf{I} + \sum_{n=1}^{\infty} \frac{\left([\mathbf{r}]^\wedge\right)^n}{n!}. \tag{23}$$

If $\mathbf{R}$ is in the neighborhood of the identity $\mathbf{I}$, we can take a first-order approximation and obtain

$$\mathbf{R} \approx \mathbf{I} + [\mathbf{r}]^\wedge. \tag{24}$$

To utilize this property in our algorithm, we need to pull the arbitrary rotation matrix back to the neighborhood of $\mathbf{I}$. In order to do this, we rewrite (2) as

$$\mathbf{R}_A\left(\mathbf{R}_{Xt}\mathbf{R}_{X0}^{-1}\right)\mathbf{R}_{X0}\mathbf{R}_B$$
$$= \left(\mathbf{R}_{Yt}\mathbf{R}_{Y0}^{-1}\right)\mathbf{R}_{Y0}\mathbf{R}_C\left(\mathbf{R}_{Zt}\mathbf{R}_{Z0}^{-1}\right)\mathbf{R}_{Z0} \tag{25}$$

where $\mathbf{R}_{\bullet t}$ represents the true value of the rotation matrix we are looking for, and $\mathbf{R}_{\bullet 0}$ means an initial value of the true rotation. If the initial value is sufficiently close to the true value, $\mathbf{R}_{\bullet t}\mathbf{R}_{\bullet 0}^{-1}$ will lie in the neighborhood of $\mathbf{I}$. Then, by substituting (24), (25) can be formulated as

$$\mathbf{R}_A\left(\mathbf{I} + [\Delta\mathbf{r}_X]^\wedge\right)\mathbf{R}_{X0}\mathbf{R}_B$$
$$\approx \left(\mathbf{I} + [\Delta\mathbf{r}_Y]^\wedge\right)\mathbf{R}_{Y0}\mathbf{R}_C\left(\mathbf{I} + [\Delta\mathbf{r}_Z]^\wedge\right)\mathbf{R}_{Z0} \tag{26}$$

where $[\Delta\mathbf{r}]^\wedge$ is the associated Lie algebra of $\mathbf{R}_{\bullet t}\mathbf{R}_{\bullet 0}^{-1}$. By rearranging (26) and ignoring the second-order small quantity $[\Delta\mathbf{r}_Y]^\wedge[\Delta\mathbf{r}_Z]^\wedge$, (26) becomes

$$\mathbf{R}_A[\Delta\mathbf{r}_X]^\wedge\mathbf{R}_{X0}\mathbf{R}_B - [\Delta\mathbf{r}_Y]^\wedge\mathbf{R}_{Y0}\mathbf{R}_C\mathbf{R}_{Z0}$$
$$-\mathbf{R}_{Y0}\mathbf{R}_C[\Delta\mathbf{r}_Z]^\wedge\mathbf{R}_{Z0} \approx -\mathbf{R}_A\mathbf{R}_{X0}\mathbf{R}_B + \mathbf{R}_{Y0}\mathbf{R}_C\mathbf{R}_{Z0}. \tag{27}$$

It can be verified that for any two 3×1 vectors $\mathbf{a}$ and $\mathbf{b}$, the following relationship holds:

$$[\mathbf{a}]^\wedge \mathbf{b} = \mathbf{a} \times \mathbf{b} = -\mathbf{b} \times \mathbf{a} = -[\mathbf{b}]^\wedge \mathbf{a}. \tag{28}$$

Hence, by rewriting (27) column by column and utilizing (28), (27) can be converted into

$$\mathbf{F}\Delta\mathbf{r} = \mathbf{c} \tag{29}$$

where

$$\Delta\mathbf{r} = \begin{bmatrix} \Delta\mathbf{r}_X^T & \Delta\mathbf{r}_Y^T & \Delta\mathbf{r}_Z^T \end{bmatrix}^T \big|_{9 \times 1} \tag{30}$$

$$\mathbf{c} = \begin{bmatrix} (-\mathbf{R}_A\mathbf{R}_{X0}\mathbf{R}_B + \mathbf{R}_{Y0}\mathbf{R}_C\mathbf{R}_{Z0})_1 \\ (-\mathbf{R}_A\mathbf{R}_{X0}\mathbf{R}_B + \mathbf{R}_{Y0}\mathbf{R}_C\mathbf{R}_{Z0})_2 \\ (-\mathbf{R}_A\mathbf{R}_{X0}\mathbf{R}_B + \mathbf{R}_{Y0}\mathbf{R}_C\mathbf{R}_{Z0})_3 \end{bmatrix}_{9 \times 1} \tag{31}$$

and $\mathbf{F}$ is defined in (32), shown at the bottom of the page, where $(\bullet)_i$ ($i = 1, 2, 3$) means to extract the ith column from the matrix in the brackets.

$$\mathbf{F} = \begin{bmatrix} -\mathbf{R}_A[(\mathbf{R}_{X0}\mathbf{R}_B)_1]^\wedge & [(\mathbf{R}_{Y0}\mathbf{R}_C\mathbf{R}_{Z0})_1]^\wedge & \mathbf{R}_{Y0}\mathbf{R}_C[(\mathbf{R}_{Z0})_1]^\wedge \\ -\mathbf{R}_A[(\mathbf{R}_{X0}\mathbf{R}_B)_2]^\wedge & [(\mathbf{R}_{Y0}\mathbf{R}_C\mathbf{R}_{Z0})_2]^\wedge & \mathbf{R}_{Y0}\mathbf{R}_C[(\mathbf{R}_{Z0})_2]^\wedge \\ -\mathbf{R}_A[(\mathbf{R}_{X0}\mathbf{R}_B)_3]^\wedge & [(\mathbf{R}_{Y0}\mathbf{R}_C\mathbf{R}_{Z0})_3]^\wedge & \mathbf{R}_{Y0}\mathbf{R}_C[(\mathbf{R}_{Z0})_3]^\wedge \end{bmatrix}_{9 \times 9}. \tag{32}$$

It will be shown in Section II-D that at least three measurements are required to make the problem solvable. At this stage, we suppose $m(m \geq 3)$ sets of measurements are performed, each of which can be formulated as an equation in the form of (29). Stacking these equations, we obtain

$$\tilde{\mathbf{F}} \Delta \mathbf{r} = \tilde{\mathbf{c}} \tag{33}$$

where

$$\tilde{\mathbf{F}} = \begin{bmatrix} \mathbf{F}_1^T & \mathbf{F}_2^T & \cdots & \mathbf{F}_m^T \end{bmatrix}^T \Big|_{9m \times 9} \tag{34}$$

$$\tilde{\mathbf{c}} = \begin{bmatrix} \mathbf{q}_1^T & \mathbf{q}_2^T & \cdots & \mathbf{q}_m^T \end{bmatrix}^T \Big|_{9m \times 1}. \tag{35}$$

Then, $\Delta \mathbf{r}$ can be solved in a least-squares sense by

$$\Delta \mathbf{r} = \left(\tilde{\mathbf{F}}^T \tilde{\mathbf{F}} \right)^{-1} \tilde{\mathbf{F}}^T \tilde{\mathbf{c}}. \tag{36}$$

The obtained $\Delta \mathbf{r}$ is subsequently used to update $\mathbf{R}_{\bullet 0}$ by

$$\mathbf{R}_{\bullet 0}^{\text{new}} = \text{Exp}\left([\Delta \mathbf{r}_i]^{\wedge} \right) \mathbf{R}_{\bullet 0}^{\text{old}} \tag{37}$$

where $\Delta \mathbf{r}_i$ $(i = X, Y, Z)$ represents the components of $\Delta \mathbf{r}$ associated with $\mathbf{X}$, $\mathbf{Y}$, and $\mathbf{Z}$, respectively.

The process iterates until the norm of $\Delta \mathbf{r}$ falls below a predefined threshold, which means that the variable converges at least to a local optimum. To ensure that the global optimum is reached, a good initial guess of the rotation matrices $\mathbf{R}_X$, $\mathbf{R}_Y$, and $\mathbf{R}_Z$ is necessary. The algorithm introduced in Section II-C1 can be used to generate a good starting point.

3) Solution to the Translational Components: The solution to the translational components is trivial when the rotational components are already solved. Rewrite (3) in the form

$$\mathbf{J} \mathbf{t} = \mathbf{p} \tag{38}$$

where

$$\mathbf{J} = \begin{bmatrix} \mathbf{R}_A & -\mathbf{I} & -\mathbf{R}_Y \mathbf{R}_C \end{bmatrix}_{3 \times 9} \tag{39}$$

$$\mathbf{t} = \begin{bmatrix} \mathbf{t}_X^T & \mathbf{t}_Y^T & \mathbf{t}_Z^T \end{bmatrix}^T \Big|_{9 \times 1} \tag{40}$$

$$\mathbf{p} = -\mathbf{t}_A - \mathbf{R}_A \mathbf{R}_X \mathbf{R}_B + \mathbf{R}_Y \mathbf{t}_C. \tag{41}$$

With m groups of data measured, we can similarly concatenate them together and have

$$\tilde{\mathbf{J}} \mathbf{t} = \tilde{\mathbf{p}} \tag{42}$$

where

$$\tilde{\mathbf{J}} = \begin{bmatrix} \mathbf{J}_1^T & \mathbf{J}_2^T & \cdots & \mathbf{J}_m^T \end{bmatrix}^T \Big|_{3m \times 9} \tag{43}$$

$$\tilde{\mathbf{p}} = \begin{bmatrix} \mathbf{p}_1^T & \mathbf{p}_2^T & \cdots & \mathbf{p}_m^T \end{bmatrix}^T \Big|_{3m \times 1}. \tag{44}$$

Hence, $\mathbf{t}$ can be simply solved by

$$\mathbf{t} = \left(\tilde{\mathbf{J}}^T \tilde{\mathbf{J}} \right)^{-1} \tilde{\mathbf{J}}^T \tilde{\mathbf{p}}. \tag{45}$$

D. Solvability Analysis

It has been clarified that at least three measurements (two robot movements) for each robot are required to solve the $\mathbf{AX} = \mathbf{XB}$ and $\mathbf{AX} = \mathbf{YB}$ problems [15], [25]. As we will see below, this is also true for the problem of solving $\mathbf{AXB} = \mathbf{YCZ}$

simultaneously. To make the problem solvable, we need to measure at least three times with the two robots moving twice (either synchronously or asynchronously). The solvability analysis will be carried out for the rotational and translational components separately.

1) Solvability of the Rotational Components: To explain the necessity of using at least three measurements to solve the rotation matrices, the first step is to investigate the number of independent variables in our unknowns.

Although a rotation matrix consists of nine components in total, only three are independent because the matrix is orthogonal, and its determinant equals one. Hence, there are nine independent variables to be identified for the three unknown rotation matrices. To determine these nine independent variables, at least nine independent equations are necessary. However, a single set of measured data only provides three independent equations since (2) describes the equivalence between two rotation matrices. In order to acquire the three unknowns, at least three sets of data are required to provide three equations in the form of (2) and thus nine independent equations.

Note that the conditions discussed above are not sufficient to uniquely determine the three unknown rotations. Configurations as described in the following lemmas will make the problem unsolvable even if three groups of measurement data are collected. In the following lemmas, the subscripts 1, 2, and 3 stand for three configurations at which each measurement is carried out.

Lemma 1: If $m = 3$ and the rotation axes of $\mathbf{R}_{A1}^T \mathbf{R}_{A2}$ and $\mathbf{R}_{A1}^T \mathbf{R}_{A3}$ are parallel or antiparallel, the rotation matrices are unsolvable.

Proof: The condition of the lemma can be expressed as

$$\mathbf{R}_{A2} = \mathbf{R}_{A1} \text{Rot}(\mathbf{a}, \alpha_1) \tag{46}$$

$$\mathbf{R}_{A3} = \mathbf{R}_{A1} \text{Rot}(\mathbf{a}, \alpha_2) \tag{47}$$

where $\mathbf{a}$ is a rotation axis, and α_1 and α_2 are rotation angles. Now, suppose $\mathbf{R}_X^0$, $\mathbf{R}_Y^0$, and $\mathbf{R}_Z^0$ are a group of solutions to the problem. It is easy to verify that

$$\mathbf{R}_X' = \text{Rot}(\mathbf{a}, \alpha) \mathbf{R}_X^0 \tag{48}$$

$$\mathbf{R}_Y' = \mathbf{R}_{A1} \text{Rot}(\mathbf{a}, \alpha) \mathbf{R}_{A1}^T \mathbf{R}_Y^0 \tag{49}$$

$$\mathbf{R}_Z' = \mathbf{R}_Z^0 \tag{50}$$

are also solutions to the problem, using the property that two coaxis rotations are commutative, i.e.,

$$\text{Rot}(\mathbf{a}, \alpha) \text{Rot}(\mathbf{a}, \alpha_i) = \text{Rot}(\mathbf{a}, \alpha_i) \text{Rot}(\mathbf{a}, \alpha). \tag{51}$$

Since α is arbitrary, there will be infinite solutions to the problem, meaning that the problem is unsolvable.

Lemma 2: If $m = 3$ and the rotation axes of $\mathbf{R}_{A1} \mathbf{R}_{A2}^T$ and $\mathbf{R}_{A1} \mathbf{R}_{A3}^T$ are parallel or antiparallel, the rotation matrices are unsolvable.

Proof: The proof of this lemma is similar to the one of Lemma 1. The condition can be expressed as

$$\mathbf{R}_{A2} = \text{Rot}(\mathbf{a}, \alpha_1) \mathbf{R}_{A1} \tag{52}$$

$$\mathbf{R}_{A3} = \text{Rot}(\mathbf{a}, \alpha_2) \mathbf{R}_{A1}. \tag{53}$$

Given $\mathbf{R}_X^0$, $\mathbf{R}_Y^0$, and $\mathbf{R}_Z^0$ as a group of solutions to the problem, we can verify that

$$\mathbf{R}_X' = \mathbf{R}_{A1}^T \mathrm{Rot}(\mathbf{a}, \alpha) \mathbf{R}_{A1} \mathbf{R}_X^0 \tag{54}$$

$$\mathbf{R}_Y' = \mathrm{Rot}(\mathbf{a}, \alpha) \mathbf{R}_Y^0 \tag{55}$$

$$\mathbf{R}_Z' = \mathbf{R}_Z^0 \tag{56}$$

are also solutions to the problem, using the property that two coaxis rotations are commutative. Since α is arbitrary, there will be infinite solutions to the problem, indicating that the problem is unsolvable.

Remark 1: $\mathbf{R}_{Ai}^T \mathbf{R}_{Aj}$ and $\mathbf{R}_{Ai} \mathbf{R}_{Aj}^T$ represent the relative rotation between the ith and jth configuration of the sensor robot expressed in the hand frame and in the base frame, respectively. Therefore, Lemmas 1 and 2 suggest that we should avoid the situation where the relative rotations between different measurement configurations of the sensor robot are coaxial.

As for $\mathbf{R}_B$ and $\mathbf{R}_C$, since (2) can also be written as

$$\mathbf{R}_B \mathbf{R}_Z^T \mathbf{R}_C^T = \mathbf{R}_X^T \mathbf{R}_A^T \mathbf{R}_Y \tag{57}$$

$$\mathbf{R}_C \mathbf{R}_Z \mathbf{R}_B^T = \mathbf{R}_Y^T \mathbf{R}_A \mathbf{R}_X \tag{58}$$

which are in the same form of (2), Lemmas 1 and 2 also stand if $\mathbf{R}_A$ is substituted with $\mathbf{R}_B$ and $\mathbf{R}_C$, respectively. Therefore, the aforementioned considerations also apply to the marker robot (due to $\mathbf{R}_C$). Besides, the relative relationship between the eye frame and the tool frame should be carefully checked as well (due to $\mathbf{R}_B$).

2) Solvability of the Translational Components: Similarly, three measurements are required to make the translational components solvable, as we have nine independent unknowns, whereas (3) provides only three independent equations.

There are also cases in which three measurements do not guarantee the solvability of the translation vectors. We will show some of them in the following lemmas.

Lemma 3: If $m = 3$ and the axes of $\mathbf{R}_{A2} \mathbf{R}_{A1}^T$ and $\mathbf{R}_{A3} \mathbf{R}_{A1}^T$ are parallel or antiparallel, the translation vectors are unsolvable.

Proof: When $m = 3$, we have

$$\tilde{\mathbf{J}} = \begin{bmatrix} \mathbf{R}_{A1} & -\mathbf{I} & -\mathbf{R}_Y \mathbf{R}_{C1} \\ \mathbf{R}_{A2} & -\mathbf{I} & -\mathbf{R}_Y \mathbf{R}_{C2} \\ \mathbf{R}_{A3} & -\mathbf{I} & -\mathbf{R}_Y \mathbf{R}_{C3} \end{bmatrix}. \tag{59}$$

$\mathbf{t}$ is solvable if and only if $Rank(\tilde{\mathbf{J}}) = 9$. Left-multiplied by

$$\begin{bmatrix} \mathbf{I} & \mathbf{0} & \mathbf{0} \\ -\mathbf{I} & \mathbf{I} & \mathbf{0} \\ -\mathbf{I} & \mathbf{0} & \mathbf{I} \end{bmatrix}$$

and right-multiplied by

$$\begin{bmatrix} \mathbf{0} & \mathbf{R}_{A1}^T & \mathbf{0} \\ -\mathbf{I} & \mathbf{0} & \mathbf{0} \\ \mathbf{0} & \mathbf{0} & -\mathbf{R}_{C1}^T \mathbf{R}_Y^T \end{bmatrix} \begin{bmatrix} \mathbf{I} & -\mathbf{I} & -\mathbf{I} \\ \mathbf{0} & \mathbf{I} & \mathbf{0} \\ \mathbf{0} & \mathbf{0} & \mathbf{I} \end{bmatrix}, \tilde{\mathbf{J}}$$

can be transformed into

$$\tilde{\mathbf{J}}' = \begin{bmatrix} \mathbf{I} & \mathbf{0} & \mathbf{0} \\ \mathbf{0} & \mathbf{R}_{A2} \mathbf{R}_{A1}^T - \mathbf{I} & \mathbf{R}_Y \mathbf{R}_{C2} \mathbf{R}_{C1}^T \mathbf{R}_Y^T - \mathbf{I} \\ \mathbf{0} & \mathbf{R}_{A3} \mathbf{R}_{A1}^T - \mathbf{I} & \mathbf{R}_Y \mathbf{R}_{C3} \mathbf{R}_{C1}^T \mathbf{R}_Y^T - \mathbf{I} \end{bmatrix}. \tag{60}$$

Since the above transformations do not change the rank of a matrix, $\tilde{\mathbf{J}}$ and $\tilde{\mathbf{J}}'$ have the same rank. Let us define

$$\mathbf{K} = \begin{bmatrix} \mathbf{R}_{A2} \mathbf{R}_{A1}^T - \mathbf{I} & \mathbf{R}_Y \mathbf{R}_{C2} \mathbf{R}_{C1}^T \mathbf{R}_Y^T - \mathbf{I} \\ \mathbf{R}_{A3} \mathbf{R}_{A1}^T - \mathbf{I} & \mathbf{R}_Y \mathbf{R}_{C3} \mathbf{R}_{C1}^T \mathbf{R}_Y^T - \mathbf{I} \end{bmatrix}. \tag{61}$$

Then, $\mathrm{Rank}(\tilde{\mathbf{J}}) = 9$ is equivalent to $\mathrm{Rank}(\mathbf{K}) = 6$.

If the axes of $\mathbf{R}_{A2} \mathbf{R}_{A1}^T$ and $\mathbf{R}_{A3} \mathbf{R}_{A1}^T$ are parallel or antiparallel, these two rotations can be decomposed with the same eigenvectors, i.e.,

$$\mathbf{R}_{A2} \mathbf{R}_{A1}^T = \mathbf{E}_A \,\mathrm{Diag}(1, e^{j\alpha_1}, e^{-j\alpha_1}) \mathbf{E}_A^T \tag{62}$$

$$\mathbf{R}_{A3} \mathbf{R}_{A1}^T = \mathbf{E}_A \,\mathrm{Diag}(1, e^{j\alpha_2}, e^{-j\alpha_2}) \mathbf{E}_A^T \tag{63}$$

where $\mathrm{Diag}(\bullet)$ means to generate a diagonal matrix from the vector in the brackets, $\mathbf{E}_A$ is an orthogonal matrix formed by eigenvectors corresponding to the eigenvalues, and α_1 and α_2 are the rotation angles of $\mathbf{R}_{A2} \mathbf{R}_{A1}^T$ and $\mathbf{R}_{A3} \mathbf{R}_{A1}^T$, respectively. Then, we have

$$\begin{aligned} \mathbf{K}_L &= \begin{bmatrix} \mathbf{R}_{A2} \mathbf{R}_{A1}^T - \mathbf{I} \\ \mathbf{R}_{A3} \mathbf{R}_{A1}^T - \mathbf{I} \end{bmatrix} \\ &= \begin{bmatrix} \mathbf{E}_A & \mathbf{0} \\ \mathbf{0} & \mathbf{E}_A \end{bmatrix} \begin{bmatrix} \mathrm{Diag}(0, e^{j\alpha_1} - 1, e^{-j\alpha_1} - 1) \\ \mathrm{Diag}(0, e^{j\alpha_2} - 1, e^{-j\alpha_2} - 1) \end{bmatrix} \mathbf{E}_A^T. \end{aligned} \tag{64}$$

It can be seen that $\mathrm{Rank}(\mathbf{K}_L) < 3$, which leads to rank deficiency of $\mathbf{K}$ and $\tilde{\mathbf{J}}$. Therefore, the translation vectors are unsolvable.

Lemma 4: If $m = 3$ and the axes of $\mathbf{R}_{C2} \mathbf{R}_{C1}^T$ and $\mathbf{R}_{C3} \mathbf{R}_{C1}^T$ are parallel or antiparallel, the translation vectors are unsolvable.

Proof: The proof is similar to that of Lemma 3, except that (64) is changed into

$$\begin{aligned} \mathbf{K}_R &= \begin{bmatrix} \mathbf{R}_Y \mathbf{R}_{C2} \mathbf{R}_{C1}^T \mathbf{R}_Y^T - \mathbf{I} \\ \mathbf{R}_Y \mathbf{R}_{C3} \mathbf{R}_{C1}^T \mathbf{R}_Y^T - \mathbf{I} \end{bmatrix} = \begin{bmatrix} \mathbf{R}_Y \mathbf{E}_C & \mathbf{0} \\ \mathbf{0} & \mathbf{R}_Y \mathbf{E}_C \end{bmatrix} \\ & \quad \begin{bmatrix} \mathrm{Diag}(0, e^{j\gamma_1} - 1, e^{-j\gamma_1} - 1) \\ \mathrm{Diag}(0, e^{j\gamma_2} - 1, e^{-j\gamma_2} - 1) \end{bmatrix} \mathbf{E}_C^T \mathbf{R}_Y^T. \end{aligned} \tag{65}$$

Lemma 5: If $m = 3$ and the axis of $\mathbf{R}_{Ai} \mathbf{R}_{A1}^T$ is parallel or antiparallel to a new axis that is constructed by rotating the axis of $\mathbf{R}_{Ci} \mathbf{R}_{C1}^T$ with $\mathbf{R}_Y$ ($i = 2, 3$), the translation vectors are unsolvable.

Proof: According to the condition of this lemma

$$\begin{aligned} \mathrm{Axis}(\mathbf{R}_{Ai} \mathbf{R}_{A1}^T) &= \pm \mathbf{R}_Y \,\mathrm{Axis}(\mathbf{R}_{Ci} \mathbf{R}_{C1}^T) \\ &= \pm \mathrm{Axis}(\mathbf{R}_Y \mathbf{R}_{Ci} \mathbf{R}_{C1}^T \mathbf{R}_Y^T) \end{aligned} \tag{66}$$

where $\mathrm{Axis}(\bullet)$ gives the unit axis of the rotation matrix in the brackets. While Lemmas 3 and 4 focus on the columns of K in (61), (66) is about the rows of K. Since the row rank and

column rank are the same for a matrix, the proof of this lemma can be formulated in the same method for proving Lemmas 3 and 4.

Remark 2: The significance of Lemmas 3 and 4 has been explained in the previous remark.

As mentioned in Remark 1, $\mathbf{R}_{Ai}\mathbf{R}_{Aj}^T$ represents the relative rotation between the ith and jth configuration of the sensor robot observed in its base frame. Meanwhile, $\mathbf{R}_Y\mathbf{R}_{Ci}\mathbf{R}_{Cj}^T\mathbf{R}_Y^T$ represents the relative rotation between the ith and jth configuration of the marker robot expressed in the base frame of the sensor robot. Therefore, Lemma 5 suggests that, observed from the base frame of the sensor robot, the relative rotation between any two configurations of the sensor robot should not be coaxial with the relative rotation between the associated two configurations of the marker robot. Otherwise, the translational vectors cannot be uniquely determined.

It is noted that the above analysis has mainly considered the case for $m = 3$ and focused on the iterative solution. For the closed-form solution, as we convert the constrained problem to an unconstrained one by introducing an intermediate variable $\mathbf{q}_{YZ}$, the minimum number of measurements required is $m = 5$ because if $m \leq 4$, the rank of $\tilde{\mathbf{W}}_{ABC}^T \tilde{\mathbf{W}}_{ABC}$ will be no greater than 16. However, the size of this symmetric matrix is 20×20. This means that $\tilde{\mathbf{W}}_{ABC}^T \tilde{\mathbf{W}}_{ABC}$ has at least four eigenvalues equal to zero. As the initial solution is determined by the eigenvector associated with the minimum eigenvalue, there will be at least four candidates for the solution, whereas we cannot distinguish the real one that solves the problem. Thus, at least five sets of data are necessary for the proposed initial solution. If only three sets of data are available, we can try to solve an initial solution by either using more complicated nonlinear solvers or by estimating the initial solution based on the mechanical dimensions. In practice, however, more than three measurement sets of data are suggested to be collected in order to reduce the effect of noise. In any case, the analysis we conducted in this section can help avoid singular configurations during the data collection process.

III. Simulation Results

To illustrate the feasibility of the proposed methods, comprehensive simulations have been carried out under different noise situations and different numbers of measurements.

A. Simulation Setup

To simplify the simulation, two six-degree-of-freedom (DOF) PUMA 560 manipulators were used to simulate the hand–eye, tool–flange, and robot–robot calibration problem, as shown in Fig. 2. The PUMA 560 kinematic parameters used in the simulation are adopted from [38]. The true values for the hand–eye, tool–flange, and robot–robot transformations used in the simulations are listed in Table I.

B. Simulation Procedure

Both the simultaneous method and the nonsimultaneous methods (the two-step and three-step methods) were tested and compared. The procedures for the simulations are as follows.
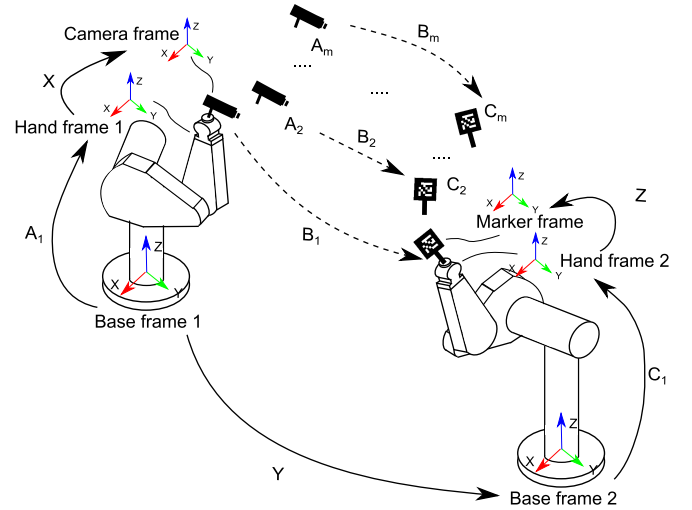

Fig. 2. Schematic diagram shows the experiment setup consisting of two Puma 560 manipulators, a tracking sensor, and a target marker to solve the hand–eye, tool–flange, and robot–robot calibration problem.

TABLE I
Setup for the Hand–Eye, Tool–Flange, and Robot–Robot Relationships in the Simulation

Rotation	Value	Translation	Value (mm)
$\mathbf{R}_X$	$\mathrm{Rot}(Z, \pi/2 + 0.01)$	$\mathbf{t}_X$	$[0\ 0\ 197]^T$
$\mathbf{R}_Y$	$\mathrm{Rot}(Z, \pi - 0.02)$	$\mathbf{t}_Y$	$[201\ 0\ 0\ 0]^T$
$\mathbf{R}_Z$	$\mathrm{Rot}(Z, \pi/4 + 0.01)$	$\mathbf{t}_Z$	$[0\ 0\ 102]^T$

For the simultaneous method, m ($m = 10, 20, \ldots, 100$) sets of data were used for the calibration. The true data for $\mathbf{A}$ and C were generated simultaneously by setting the sensor robot and the marker robot to a random configuration within their respective workspace. Additional care was given in ensuring that the marker was kept inside the measuring scope of the sensor (otherwise, this pair of configurations would be rejected). The true data for $\mathbf{B}$ were calculated by applying $\mathbf{AXB} = \mathbf{YCZ}$. In order to simulate the real scenarios, noise was introduced in all generated data. The initial solution proposed in this paper was employed to produce a starting point by using the first ten sets of data only and then followed by the iterative algorithm that generated the final solutions for $\mathbf{X}$, $\mathbf{Y}$, and $\mathbf{Z}$.

For the two-step method, the procedure of generating data can be divided into two steps. First, the marker robot was set to a suitable configuration and kept immobile, resulting in a static $\mathbf{C}$. At the same time, running the sensor robot in different configurations and calculating the corresponding relationship between the sensor and the marker collected m effective data for $\mathbf{A}$ and $\mathbf{B}$. By using the $\mathbf{AX} = \mathbf{XB}$ (notice that $\mathbf{A}$ and $\mathbf{B}$ in this equation are not of the same meaning as mentioned above) algorithm introduced in [17], $\mathbf{X}$ was obtained. Second, the sensor robot was kept static, and m effective data for $\mathbf{B}$ and $\mathbf{C}$ were generated. $\mathbf{Y}$ and $\mathbf{Z}$ were then calculated by using the $\mathbf{AX} = \mathbf{YB}$ method provided by Li *et al.* [28].

TABLE II
THREE LEVELS OF NOISE INJECTED INTO THE MEASURED DATA

Noise Level	Rotational noise (°)	Translational noise (mm)
Low	$\theta(\mathbf{R}_A) \sim \mathcal{U}(-0.025, 0.025)$	$\|\mathbf{t}_A\| \sim \mathcal{U}(-0.1, 0.1)$
	$\theta(\mathbf{R}_B) \sim \mathcal{U}(-0.05, 0.05)$	$\|\mathbf{t}_B\| \sim \mathcal{U}(-0.2, 0.2)$
	$\theta(\mathbf{R}_C) \sim \mathcal{U}(-0.025, 0.025)$	$\|\mathbf{t}_C\| \sim \mathcal{U}(-0.1, 0.1)$
Medium	$\theta(\mathbf{R}_A) \sim \mathcal{U}(-0.1, 0.1)$	$\|\mathbf{t}_A\| \sim \mathcal{U}(-0.5, 0.5)$
	$\theta(\mathbf{R}_B) \sim \mathcal{U}(-0.2, 0.2)$	$\|\mathbf{t}_B\| \sim \mathcal{U}(-1, 1)$
	$\theta(\mathbf{R}_C) \sim \mathcal{U}(-0.1, 0.1)$	$\|\mathbf{t}_C\| \sim \mathcal{U}(-0.5, 0.5)$
High	$\theta(\mathbf{R}_A) \sim \mathcal{U}(-0.25, 0.25)$	$\|\mathbf{t}_A\| \sim \mathcal{U}(-1, 1)$
	$\theta(\mathbf{R}_B) \sim \mathcal{U}(-0.5, 0.5)$	$\|\mathbf{t}_B\| \sim \mathcal{U}(-2, 2)$
	$\theta(\mathbf{R}_C) \sim \mathcal{U}(-0.25, 0.25)$	$\|\mathbf{t}_C\| \sim \mathcal{U}(-1, 1)$

Fig. 3. Average accuracy for the three methods under low-level noise by using a different number of measurements.
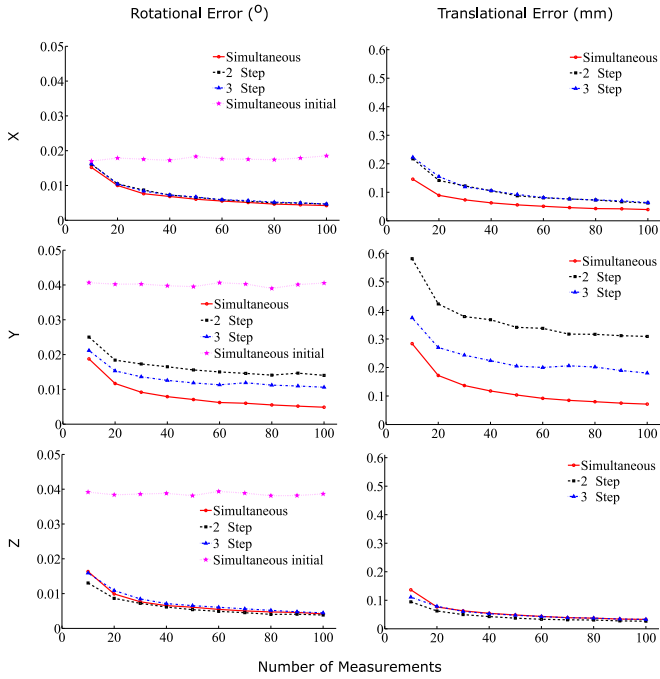

Fig. 4. Average accuracy for the three methods under medium-level noise by using a different number of measurements.

For the three-step method, the first step of the procedure was the same as the two-step method. However, in the second step, only **Z** was calculated by using the same $\mathbf{AX} = \mathbf{XB}$ algorithm. Finally, with solutions of **X** and **Z**, **Y** was computed by estimating the optimal solution to conform with the data of the previous two steps.

C. Noise Injected Into the Data

Three different levels of noise, namely "low level," "medium level," and "high level," as listed in Table II, were injected into the simulation data in order to investigate the performance of the proposed methods under different levels of disturbance. Similar to the approach adopted in [25] and [39], uniformly distributed noise was added to rotation and translation. The noise injected is

$$\mathbf{R}_i^{\text{noise}} = \mathbf{R}_i^{\text{true}} \text{Rot}(\mathbf{a}, \theta(\mathbf{R}_i)) \tag{67}$$

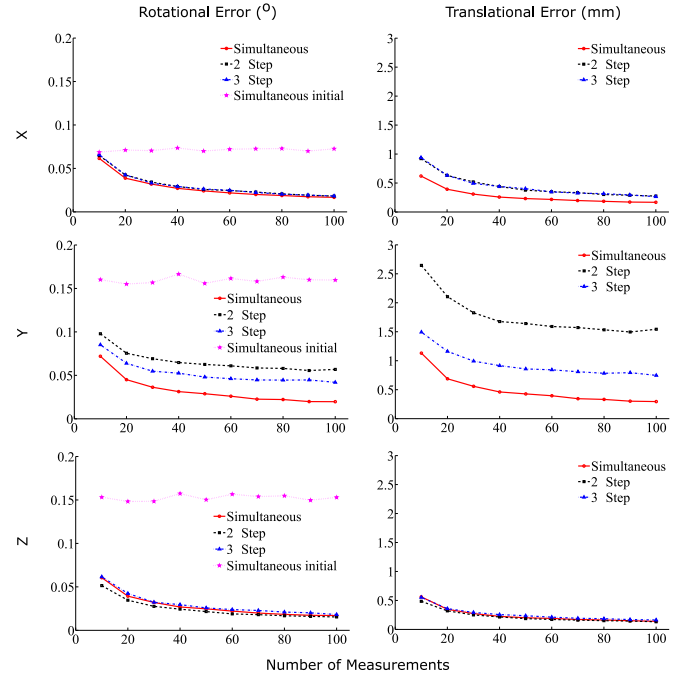$$\mathbf{t}_i^{\text{noise}} = \mathbf{t} + \|\mathbf{t}_i\|\mathbf{b} \tag{68}$$

where **a** and **b** are random unit 3-D directions, $\theta(\mathbf{R}_i)$ and $\|\mathbf{t}_i\|$ are amplitude of rotational noise and translational noise, and the subscript i indicates **A**, **B**, and **C**. Commercial industrial robots' position accuracy is usually about 1–2 mm; if calibrated, this performance can be improved to submillimeter level [34], [35]. Thus, the injected noise generally represents the real-world situation. In addition, regarding the fact that the measured data from hand-mounted sensors are more fragile to noise, it is assumed that $\mathbf{B}_i$ is corrupted by noise with greater variances.

D. Results

Figs. 3–5 show the results of the simulations under low, medium, and high level of noise, respectively.

In each figure, the rotational errors and the translational errors of the three methods are depicted with respect to the number of datasets. The solid line with circle markers, the dashed line with square markers, and the dashed-dotted line with triangle markers denote the results of simultaneous two-step and three-step methods, respectively. The rotational errors of the proposed initial solution are also presented by the dotted line with pentagram markers. Five hundred trials were carried out with each method under the same number of measurements but with different random noises to get an average evaluation. In all the results, the rotational error $^S e_{r,i}$ and the translational error $^S e_{t,i}$ are defined in

$$^S e_{r,i} = \theta(\hat{\mathbf{R}}_i \bar{\mathbf{R}}_i^{-1}) \tag{69}$$

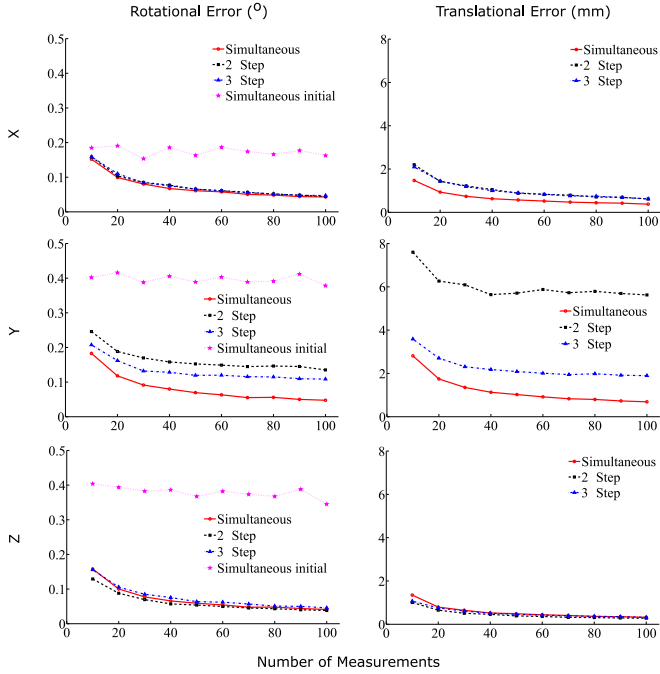$$^S e_{t,i} = \|\hat{\mathbf{t}}_i - \bar{\mathbf{t}}_i\| \tag{70}$$

Fig. 5. Average accuracy for the three methods under high-level noise by using a different number of measurements.
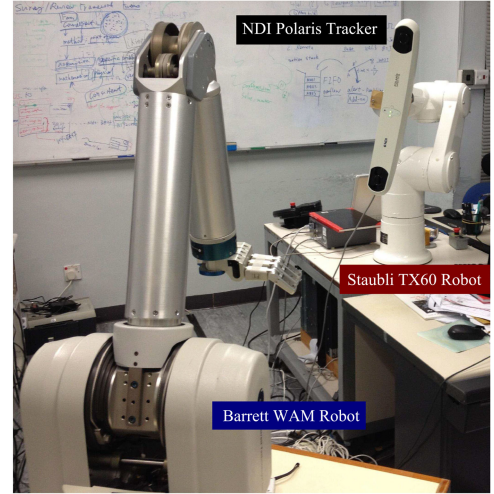

Fig. 6. Experiment is carried out by using a Staubli TX60 robot and a Barrett WAM robot. An NDI Polaris optical tracker is mounted to the Staubli robot to track a reflective marker (invisible from current camera angle) that is mounted to the WAM robot.

where the left superscript $^S\bullet$ stands for the simulation results, $\theta(\bullet)$ stands for the calculation of the rotational angle, $\hat{\bullet}$ and $\bar{\bullet}$ stand for estimated and true values of the rotation matrices $\mathbf{R}_i$ and translation vectors $\mathbf{t}_i$, and i stands for the unknown $\mathbf{X}$, $\mathbf{Y}$, and $\mathbf{Z}$.

In these figures, all three methods are seen as capable of finding the unknown $\mathbf{X}$, $\mathbf{Y}$, and $\mathbf{Z}$ under the three noise levels. However, the accuracy of each solution decreases with the increase of noise. All the methods demonstrate trends of increasing accuracy with increasing number of datasets under each noise level. It is observed that a significant slowdown in the ratio of accuracy improvement occurs at around 30 sets of data.

With respect to the rotational error, the three methods perform evenly in the accuracy of $\mathbf{Z}$. However, the simultaneous method slightly outperforms in the accuracy of $\mathbf{X}$ and significantly in the accuracy of $\mathbf{Y}$ than the other two nonsimultaneous methods.

The results of the translational part are similar to the rotational ones. The simultaneous method performs as well as the other two methods in the accuracy of $\mathbf{Z}$ but achieves a significant improvement in the accuracy of $\mathbf{X}$ and $\mathbf{Y}$.

As for the proposed initial solution for the simultaneous method, the accuracy of the results is not as good as the other three methods. The reason for this has been discussed in Section II-C1. Since only ten sets of data are used to produce an initial solution in all the simulations, the accuracy does not increase along with the total number of measurements. It is also noted that the initial solution of $\mathbf{X}$ is better than $\mathbf{Y}$ and $\mathbf{Z}$ because an intermediate term $\mathbf{q}_{YZ}$ is used in the algorithm that introduces some inconsistency due to noise. Nevertheless, the proposed initialization algorithm provides a good initial estimation for the further iterative steps.

IV. EXPERIMENT RESULTS

A. Experiment Setup

Besides the simulation, ample real-world experiments have been conceived and carried out under different configurations to evaluate the proposed methods. As shown in Fig. 6, the experiments involved a Staubli TX60 robot (six DOFs, averaged repeatability 0.02 mm), a Barrett WAM robot (four DOFs, averaged repeatability 0.05 mm), and an NDI Polaris optical tracker (RMS repeatability 0.10 mm). The optical tracker was mounted to the last link of the Staubli robot, referred to as the sensor robot. The corresponding reflective marker was mounted to the last link of the WAM robot, referred to as the marker robot.

To achieve the simultaneous calibration, the two manipulators were programmed to move to a set of 300 random positions under which the optical tracker tracked the marker each time when both of the two manipulators finished their motions. The homogeneous transformations of the sensor and marker robots' hand frames with respect to their base frames ($\mathbf{A}$s and $\mathbf{C}$s, respectively) and the homogeneous transformations of the marker with respect to the optical tracker ($\mathbf{B}$s) were calculated at the same time. In the two-step and three-step calibrations, one of the robots was held static while the other one carried out aforementioned set of random movements by turn. This results in two data acquisition procedures, which produces $\mathbf{A}$s and $\mathbf{B}$s for the first procedure and $\mathbf{C}$s and $\mathbf{B}$s for the second one.

All the calibration data were collected under three different system configurations: at approximately 1.7 m, 2.2 m, and 2.7 m distances between the origins of the sensor and marker robots' base frames. These distances are referred to as *near*, *medium*, and *far* configurations, respectively. In order to compare these three distances under the same condition, we set the random motions of the robots to be identical for the three configurations.

Because the ground truths for $\mathbf{X}$, $\mathbf{Y}$, and $\mathbf{Z}$ are not available in the experiment setup, the rotational errors ($^E e_{r,i}$) and

TABLE III
DATA MISSING AND OUTLIER RATIOS IN RAW DATA PREPROCESSING

	$\mathbf{AXB} = \mathbf{YCZ}$	$\mathbf{AX} = \mathbf{XB}^{\dagger}$	$\mathbf{AX} = \mathbf{YB}$
	Missing Ratio(%)	Outlier Ratio(%)		
Near	58.33 | 1.60	52.67 | 3.52	20.67 | 0
Medium	34.33 | 8.63	31.67 | 8.29	10.33 | 2.60
Far	28.67 | 24.30	24.33 | 14.10	14.00 | 5.43

† Averaged ratio for hand–eye calibrations in the two-step and
three-step methods.

TABLE IV
ELAPSE TIME OF RANSAC FOR SIMULTANEOUS METHOD

	Min	Max	Median	Mean	Std
Near (s)	0.5063	1.1606	0.6468	0.6656	0.1060
Medium (s)	0.6769	1.3778	0.8647	0.8797	0.1201
Far (s)	0.7747	1.6351	1.0217	1.0716	0.1863

This table shows the results of 100 repetitions of independent experiments after data alignment.

translational errors ($^{E}e_{t,i}$) for the ith measurement are defined in

$$\mathbf{E}_i = (\mathbf{A}_i \hat{\mathbf{X}} \mathbf{B}_i)(\hat{\mathbf{Y}} \mathbf{C}_i \hat{\mathbf{Z}})^{-1} \qquad (71)$$

$$^{E}e_{r,i} = \theta(\mathbf{R}_{Ei}) \qquad (72)$$

$$^{E}e_{t,i} = \|\mathbf{t}_{Ei}\| \qquad (73)$$

where $\mathbf{E}_i$ stands for the error matrix of the simultaneous calibration method for the ith measurement, the left superscript $^{E}\bullet$ stands for the experiment results, $\theta(\bullet)$ stands for the calculation of the rotational angle, and $\hat{\bullet}$ stands for the calculated estimation of the unknowns.

B. Raw Data Preprocessing

Due to the random nature of the robots' motion in this experiment, the optical tracker cannot be completely consistent in tracking the marker during the trials. Missing data from $\mathbf{B}$s should first be processed out from calibration, as well as the corresponding $\mathbf{A}$s and $\mathbf{C}$s. The data that are missing ratios for the experiments under different configurations for simultaneous and nonsimultaneous methods are listed in Table III.

Unlike the simulation data, the experimental data usually suffer from environmental uncertainties, such as unpredictable sensor noises and synchronization problems. These outliers, which influence the real performance of the calibration methods, can be excluded by using a random sample consensus (RANSAC) processing. The input of the RANSAC is from the output data alignment processing. The data alignment processing is to eliminate missing data from As, Bs, and Cs and to synchronize the timeline for the rest of the data. The RANSAC algorithm provides a more robust solution for different noises than a simple thresholding method. Additionally, the RANSAC processing provides a more adaptive solution for different models (simultaneous, two-step, three-step) than a simple thresholding method.

For the simultaneous method, we use (71) as an error criterion of RANSAC to find the outliers after the data alignment. For the nonsimultaneous methods, the error criteria of RANSAC are defined in

$$^{HE}\mathbf{E}_i = (\mathbf{A}_i \hat{\mathbf{X}})(\hat{\mathbf{X}} \mathbf{B}_i)^{-1} \qquad (74)$$

$$^{RT}\mathbf{E}_i = (\mathbf{A}_i \hat{\mathbf{X}})(\hat{\mathbf{Y}} \mathbf{B}_i)^{-1} \qquad (75)$$

where $^{HE}\mathbf{E}_i$ stands for the error matrix of the hand–eye calibration method, and $^{RT}\mathbf{E}_i$ stands for the error matrix of robot–world and tool–flange calibration method. The rotational and

translational errors are calculated in the same manner as defined in (72) and (73).

The main parameters of the RANSAC are false alarm rate (ϵ), sample size, and rotational and translational thresholds. The false alarm rate, which is set to 0.01 for current application, is the probability that the algorithm through all the iteration will never sample a minimum sampling set of data that contains only inliers. In other words, the probability of at least one outlier through all the iteration will be $1 - \epsilon$, viz. 99% for this project. This is a reasonable selection for RANSAC, as [40] uses $\epsilon = 0.001$ as a default value in the project.

Sample size is the data size for the minimum sampling set of data. Since the minimum sampling set of data will be used to fit the model and this operation needs to be repeated a large number of times, therefore the sample size should be a very small number. Since the three-step and two-step need at least six datasets (see Section II-B for details), the sample size is set to be 6 in this project.

The RANSAC aims to eliminate only erroneous outliers. It does not try to tune the data to provide better performance. After observation, we found that 6 mm and $1.5°$ are reasonable thresholds to serve the aforementioned purposes in this paper. Additionally, the algorithm parameters remain the same for all calibration methods and all system configurations, which makes it possible to fairly compare the performances. The outlier ratios of the experiments under different configurations for simultaneous and nonsimultaneous methods are also listed in Table III.

Time consumption of the RANSAC processing for the simultaneous method has been thoroughly investigated on a Windows 8.1 64-bit platform with an Intel Core2 Duo Core P8600 processor at 2.40 GHz and 8 GB of RAM. After the data alignment, RANSAC processing has been independently conducted 100 times under the near, medium, and far configurations, respectively. The statistics of the elapse times of the three configurations have been tabulated into columns of minimum, maximum, median, mean, and standard deviation, as shown in Table IV.

C. Results

To demonstrate the superiority of the simultaneous method in the real experimental scenarios, a fivefold cross-validation approach is implemented 200 times for all the calibration methods under all system configurations. For a simultaneous method, after data alignment and RANSAC processing, 80% of the remaining data are randomly selected to calculate $\mathbf{X}$, $\mathbf{Y}$, and $\mathbf{Z}$, and 20% are used as test data to evaluate the performance by (71), (72), and (73). For two-step and three-step methods, the

same test data from the simultaneous method are used to evaluate their performances after calculating the unknowns by each method.

Range is one of the most influential effects in the real practice of the proposed methods. In Section III, the effect caused by range difference is simulated by adding different levels of noises to the tracked data $\mathbf{B}$s. However, real experiments usually are subjected to more complicated uncertainties than synthetic data. By varying the distance between the origins of the base frames of the two robots, the range influence is investigated under different calibration methods.

The rotational and translational errors of the 200 rounds of fivefold cross-validation for the three proposed methods at three different ranges are first evaluated by (71)–(73). In Fig. 7, the evaluated errors of 200 rounds of fivefold cross-validation for the three proposed methods at three different ranges are shown as box plots. Left-tail paired-samples t-tests have been conducted to compare the performance of the simultaneous method versus that of the two-step and three-step methods, respectively. The results indicate that the rotational and translational errors from the simultaneous method are significantly smaller than those of the two-step and three-step methods. Only two nonsignificant results exist in the rotational performances at medium and far ranges when comparing the simultaneous method with the three-step one. Nevertheless, the simultaneous method outperforms the nonsimultaneous ones in terms of translation error at all ranges.

V. DISCUSSION

A. Accuracy

Generally, the simultaneous method achieves better accuracy than the nonsimultaneous methods, as shown in Figs. 3–5 and 7. For the solutions of $\mathbf{X}$ and $\mathbf{Z}$, the results of simultaneous method are as good as the other two. However, for the solution of $\mathbf{Y}$, which is the transformation between the base frames of the two mobile robots, the simultaneous method shows significantly better results.

It is noted that the simultaneous and nonsimultaneous methods take two different approaches to address the strong nonlinear coupling property of $\mathbf{X}$, $\mathbf{Y}$, and $\mathbf{Z}$ shown in the original problem. The simultaneous method is capable of better balancing the errors within the three unknowns. The nonsimultaneous methods solve the unknowns one by one, which leads to error propagation and accumulation. This is shown by the poor performance of two-step and three-step when calculating $\mathbf{Y}$. By contrast, the simultaneous one improves the overall accuracy from a global perspective.

B. Convergence Speed

Convergence speed of the iterative algorithm is another critical concern besides the accuracy performance. In the following, the convergence speed is investigated by analyzing the required iterations for convergence during the experiments.

Fig. 8 shows frequency statistics of the iteration steps of the simultaneous method under all experimental configurations
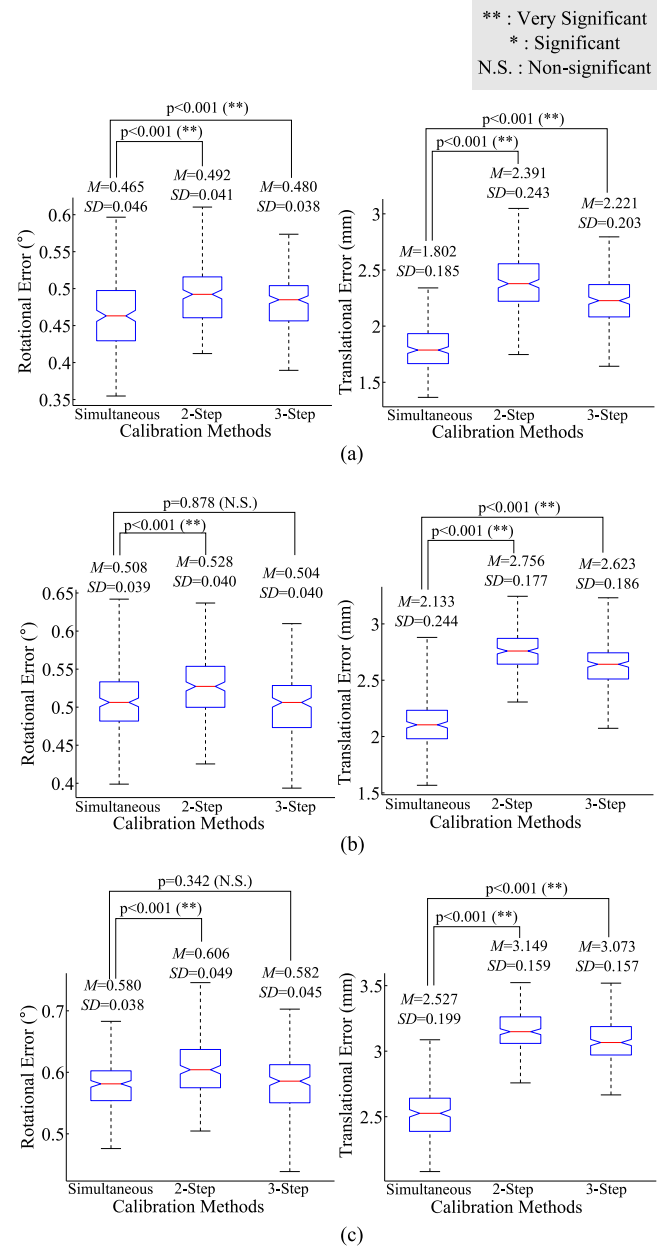

Fig. 7. Results of 200 rounds of fivefold cross-validation and left-tail paired-samples t-test at the near, medium, and far ranges. The box plots show the rotational and translational error distributions for three methods at three ranges. $**$, $*$, and $N.S.$ stand for very significant at 99% confidence level, significant, and nonsignificant at 95% confidence level, respectively.

across 200 rounds of fivefold cross-validation. The stopping criteria is $||\Delta\mathbf{r} \leq 10^{-10}||$, in which $\Delta\mathbf{r}$ is defined in (30). For the far, medium, and near ranges, the median iteration numbers are $7, 7$, and 8, respectively. Because the majority of the iteration numbers are all distributed below 8, there is strong indication of high efficiency and stability with the proposed simultaneous method.

C. Initial Solution

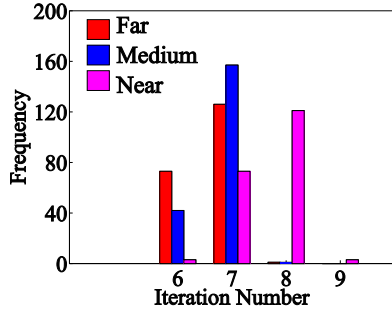Because of the iterative nature of the proposed simultaneous method, its performance may highly depend on the

Fig. 8. Frequency statistics of the iteration number under three different experimental ranges. The vertical axis represents the number of cases in which the iteration number is equal to the value shown in the horizontal axis among the 200 rounds of experiments. The red, blue, and magenta bars represent far, medium, and near ranges, respectively.
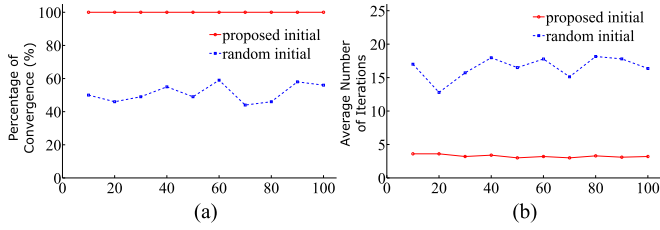

Fig. 9. Result comparison between the simultaneous iterative method using the proposed initial solution and the one using random initial guess.

initial solution. To investigate the feasibility of the proposed quaternion-based method for the initial solution, we carried out a simulation in which the iterative method was provided with the initial solution obtained by the proposed closed-form method and in which the initial solution was generated randomly. The simulation was run 500 times, and the convergence rate and the average number of iteration steps in the converging cases are depicted in Fig. 9. It can be seen that the convergence rate of the iterative method with the proposed initial solution is always 100% , while utilizing random initial guesses yields a convergence rate of only 50% approximately. In the converging cases, the method using the proposed initial solution also evinces a faster converging speed than the one adopting the random initial guess, with an average number of iteration steps about one-fifth of the latter one. In a word, the proposed initial solution provides a good starting point for the successive iterative method.

D. Comparison With Standard Nonlinear Optimization Algorithms

We also compared the proposed algorithm with standard nonlinear optimization algorithms. As the solution to the translational components is quite straightforward, we only compared the solution to the rotational components. In order to use the standard nonlinear optimization algorithms, we formulated the simultaneous calibration problem as

$$\min \sum_{i=1}^{m} \|\mathbf{R}_{Ai}\mathbf{R}_X\mathbf{R}_{Bi} - \mathbf{R}_Y\mathbf{R}_{Ci}\mathbf{R}_Z\|_F^2 \qquad (76)$$

TABLE V
ACCURACY COMPARISON BETWEEN THE PROPOSED ALGORITHM AND THE INTERIOR-POINT ALGORITHM[1]

Error[2]	Proposed Algorithm	Interior-Point Algorithm	
		Without UPHM[3]	With UPHM[3]
$\mathbf{R}_X$	0.042644	0.042641	0.042641
$\mathbf{R}_Y$	0.047902	0.047878	0.047878
$\mathbf{R}_Z$	0.042055	0.042032	0.042032
$\mathbf{t}_X$	0.395381	0.395381	0.395381
$\mathbf{t}_Y$	0.715399	0.715399	0.715399
$\mathbf{t}_Z$	0.337169	0.337169	0.337169

[1] This table shows the average results of 500 times of independent simulations with 100 sets of measurement data.
[2] The unit is *degree* for rotational error and mm for translational error.
[3] UPHM stands for user-provided Hessian matrix.

$$s.t.\,\mathbf{R}_X^T\mathbf{R}_X - \mathbf{I} = \mathbf{0},\ |\mathbf{R}_X| - 1 = 0 \qquad (77)$$

$$\mathbf{R}_Y^T\mathbf{R}_Y - \mathbf{I} = \mathbf{0},\ |\mathbf{R}_Y| - 1 = 0 \qquad (78)$$

$$\mathbf{R}_Z^T\mathbf{R}_Z - \mathbf{I} = \mathbf{0},\ |\mathbf{R}_Z| - 1 = 0 \qquad (79)$$

where $\|\bullet\|_F$ stands for the Frobenius norm of a matrix, and $|\bullet|$ denotes the determinant of a matrix. This is an optimization problem with nonlinear constraints; thus, we used the *fmincon* function provided by MATLAB 7.14, which supports four different options of algorithms, including *interior-point*, *active-set*, *sqp*, and *trust-region-reflective*, to solve this optimization problem. Since the *trust-region-reflective* algorithm does not accept nonlinear constraints, only the first three algorithms can be used. However, we found that the *active-set* and the *sqp* algorithms could not converge to a feasible solution in our tests. Therefore, we will present the comparison results with only the *interior-point* algorithm.

In our tests, we compared the proposed algorithm, the *interior-point* algorithm without UPHM (user-provided Hessian matrix), and the *interior-point* algorithm with UPHM. The initial points required by these three algorithms were all generated by the quaternion-based solution proposed in Section II-C. The simulation setup was set similar to the case with high-level noise described in Section III. Each algorithm was carried out 500 times to obtain an average evaluation. Table V shows the comparison in accuracy between the proposed algorithm and the other two algorithms. It can be seen that the accuracy of the three algorithms is close, with a difference no greater than $10^{-4\circ}$ in terms of the rotational error and 10^{-6} mm in terms of the translational error. This proves that the linear approximation adopted in our algorithm does not affect the accuracy of the optimization.

The average iteration steps and runtime of each algorithm are compared in Fig. 10. It can be seen that the number of iteration steps required by the proposed algorithm (about four iteration steps) is only a little greater than the *interior-point* algorithm with UPHM, and much less than the *interior-point* algorithm without UPHM. The runtime of the proposed algorithm (about 0.06 s) significantly outperforms the other two. If the user does
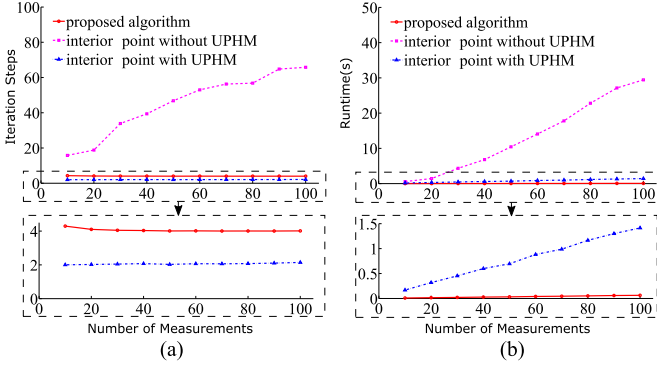
Fig. 10. Efficiency comparison between the proposed algorithm and the interior-point algorithm. UPHM stands for user-provided Hessian matrix.

not provide the Hessian matrix, the *interior-point* algorithm will compute it by a finite-difference approximation. Even when the Hessian matrix is explicitly provided, the calculation of the Hessian matrix is still burdensome both in computation time and in memory allocation and makes the *interior-point* algorithm less efficient than the proposed algorithm.

E. Efficiency in Practice

The simultaneous method is more efficient than the other two methods when we are solving the real problems in practice.

First, the data collection processes of the nonsimultaneous methods are more complex and time consuming than the simultaneous one. Suppose we have the same sets of calibration configurations for the robots to fulfill, the time required for the nonsimultaneous methods are almost twice that of the simultaneous one because the robots have to move sequentially in the nonsimultaneous methods.

Second, since accuracy improves with the increase of measurement data, and that the simultaneous method is more accurate than the nonsimultaneous ones with the same amount of data, more data are required for the nonsimultaneous methods in order to achieve the same accuracy as the simultaneous method.

F. From Paired-Robot to Multirobot

When more than two robots are working cooperatively on the same task, the calibration has to be extended from paired-robot to multirobot. This can be achieved in two approaches: a star-type topology approach and a ring-type topology approach. In either case, the problem of inconsistency among the calibration results will be encountered.

To show this inconsistency, we choose a simple three-robot calibration problem as an example. In the star-type topology, one robot can be chosen as an intermediate robot. Two other robots can be separately calibrated with respect to the intermediate robot. As a result, the inconsistency will be shown in the unknown $\mathbf{X}$ or $\mathbf{Z}$ of the intermediate robot. In the ring-type topology, the involved robots can be formed into a loop and the calibration between each adjacent paired-robot can be performed. In this case, a loop-closing problem will emerge

when calibrating the last paired-robot, therefore creating inconsistency in the initial robot.

The aforementioned problem is nontrivial for the multirobot applications to gain accuracy as well as consistency. A global refining process such as the bundle adjustment method [41] can be used to find the optimal solutions for this problem. This topic is beyond the scope of this paper and will be investigated elsewhere.

VI. CONCLUSION

We have proposed a simultaneous hand–eye, tool–flange, and robot–robot calibration method, which is essential in the application of multirobot cooperative manipulation. The problem was formulated as solving a matrix equation $\mathbf{AXB} = \mathbf{YCZ}$. A closed-form initial value estimation was originally derived based on the algebra of quaternions for the simultaneous method. Then, a linear approximation iterative algorithm was put forward to efficiently and accurately converge to the true solution based on the initial estimation. The solvability of the proposed method was analyzed, showing that at least three measurements were required to uniquely determine a solution. Additionally, the outstanding performance of the proposed algorithm over standard nonlinear optimization algorithms was demonstrated. To show the feasibility and superiority of the simultaneous method, two nonsimultaneous methods were used for comparison. Comprehensive simulations and experiments were carried out to demonstrate the superiority of the proposed simultaneous method over nonsimultaneous ones in terms of average accuracy and efficiency.

In our future work, the inconsistency issue in the extension from paired-robot to multirobot discussed in Section V-F will be further investigated. In addition, investigation on using partial measurement data and extension to multiple manipulators will be performed.

APPENDIX A
AMBIGUITY PROBLEM IN DERIVING THE CLOSED-FORM SOLUTION BASED ON QUATERNION

The proposed quaternion-based algorithm for the solution of rotational components in Section II-C1 is to solve $\mathbf{q}_{XYZ}$ from (13). It is known that a quaternion $\mathbf{q}$ that multiplies itself by -1 corresponds to the same rotation matrix $\mathbf{R}$, i.e., we have two candidate quaternions, $\mathbf{q}$ and $-\mathbf{q}$, to relate to a given rotation matrix. Suppose we set a rule that only the quaternion whose first nonzero component is nonnegative is considered when deriving a quaternion from a rotation, which is common in dealing with the sign ambiguity. For a single measurement, we still have two possible formulations

$$\begin{bmatrix} \mathbf{W}_{AB,i} & \mathbf{W}_{C,i} \end{bmatrix} \begin{bmatrix} \mathbf{q}_X \\ \mathbf{q}_{YZ} \end{bmatrix} = 0 \qquad (80)$$

$$\begin{bmatrix} \mathbf{W}_{AB,i} & -\mathbf{W}_{C,i} \end{bmatrix} \begin{bmatrix} \mathbf{q}_X \\ \mathbf{q}_{YZ} \end{bmatrix} = 0 \qquad (81)$$

depending on the relationships among the rotations $\mathbf{R}_A$, $\mathbf{R}_B$, $\mathbf{R}_C$, $\mathbf{R}_X$, $\mathbf{R}_Y$, and $\mathbf{R}_Z$. If we have only one measurement in

total, this ambiguity does not affect the final solution because the solution to (80), denoted as $\mathbf{q}_{XYZ} = [\mathbf{q}_X^T \ \mathbf{q}_{YZ}^T]^T$, and the solution to (81), denoted as $\mathbf{q}'_{XYZ} = [\mathbf{q}_X^T \ -\mathbf{q}_{YZ}^T]^T$, render the same rotation. Therefore, no matter which formulation we have adopted, the obtained rotation matrix is always correct. However, this ambiguity leads to problems when we have multiple measurements (which is the case in a real calibration). Let us take two measurements for example. The true solution can correspond to any of the following four formulations:

$$\begin{bmatrix} \mathbf{W}_{AB,1} & \mathbf{W}_{C,1} \\ \mathbf{W}_{AB,2} & \mathbf{W}_{C,2} \end{bmatrix} \begin{bmatrix} \mathbf{q}_X \\ \mathbf{q}_{YZ} \end{bmatrix} = 0 \tag{82}$$

$$\begin{bmatrix} \mathbf{W}_{AB,1} & -\mathbf{W}_{C,1} \\ \mathbf{W}_{AB,2} & \mathbf{W}_{C,2} \end{bmatrix} \begin{bmatrix} \mathbf{q}_X \\ \mathbf{q}_{YZ} \end{bmatrix} = 0 \tag{83}$$

$$\begin{bmatrix} \mathbf{W}_{AB,1} & -\mathbf{W}_{C,1} \\ \mathbf{W}_{AB,2} & -\mathbf{W}_{C,2} \end{bmatrix} \begin{bmatrix} \mathbf{q}_X \\ \mathbf{q}_{YZ} \end{bmatrix} = 0 \tag{84}$$

$$\begin{bmatrix} \mathbf{W}_{AB,1} & \mathbf{W}_{C,1} \\ \mathbf{W}_{AB,2} & -\mathbf{W}_{C,2} \end{bmatrix} \begin{bmatrix} \mathbf{q}_X \\ \mathbf{q}_{YZ} \end{bmatrix} = 0. \tag{85}$$

The solutions to (82) and (83) are essentially equivalent to the solutions to (84) and (85), respectively. However, the solutions to (82) and (84) are absolutely different from the solutions to (83) and (85), and they correspond to different rotations. It is noted that only one set of solutions can lead to the true rotation. The problem is that we do not know which formulation the true rotation belongs to in advance, resulting in the sign ambiguity problem we addressed in the paper.

This sign ambiguity issue has also been mentioned in [26].

Acknowledgment

References

[1] C. P. Tang, R. M. Bhatt, M. Abou-Samah, and V. Krovi, "Screw-theoretic analysis framework for cooperative payload transport by mobile manipulator collectives," *IEEE/ASME Trans. Mechatronics*, vol. 11, no. 2, pp. 169–178, Apr. 2006.

[2] A. C. Lehman, K. A. Berg, J. Dumpert, N. A. Wood, A. Q. Visty, M. E. Rentschler, S. R. Platt, S. M. Farritor, and D. Oleynikov, "Surgery with cooperative robots," *Comput. Aided Surg.*, vol. 13, no. 2, pp. 95–105, 2008.

[3] T. Fisher, A. Hamed, P. Vartholomeos, K. Masamune, G. Tang, H. Ren, and Z. T. H. Tse, "Intraoperative magnetic resonance imaging-conditional robotic devices for therapy and diagnosis," *Proc. Inst. Mech. Eng. H, J. Eng. Med.*, vol. 228, no. 3, pp. 303–318, 2014.

[4] A. Hamed, S. C. Tang, H. Ren, A. Squires, C. Payne, K. Masamune, G. Tang, J. Mohammadpour, and Z. T. H. Tse, "Advances in haptics, tactile sensing, and manipulation for robot-assisted minimally invasive surgery, noninvasive surgery, and diagnosis," *J. Robot.*, vol. 2012, art. no. 412816, 2012.

[5] J. Wang, H. Ren, and M. Q.-H. Meng, "A preliminary study on surgical instrument tracking based on multiple modules of monocular pose estimation," in *Proc. IEEE 4th Annu. Int. Conf. Cyber Technol. Autom. Control Intell. Syst.*, 2014, pp. 146–151.

[6] J. Wang, H. Ren, and M. Meng, "Towards occlusion-free surgical instrument tracking: A modular monocular approach and an agile calibration

method," *IEEE Trans. Autom. Sci. Eng.*, vol. 12, no. 2, pp. 588–595, Apr. 2015.

[7] P. Mahacek, C. A. Kitts, and I. Mas, "Dynamic guarding of marine assets through cluster control of automated surface vessel fleets," *IEEE/ASME Trans. Mechatronics*, vol. 17, no. 1, pp. 65–75, Feb. 2012.

[8] H. Bai and J. T. Wen, "Cooperative load transport: A formation-control perspective," *IEEE Trans. Robot.*, vol. 26, no. 4, pp. 742–750, Aug. 2010.

[9] H. Ren, C. M. Lim, J. Wang, W. Liu, S. Song, Z. Li, G. Herbert, Z. T. H. Tse, and Z. Tan, "Computer-assisted transoral surgery with flexible robotics and navigation technologies: A review of recent progress and research challenges," *Crit. Rev. Biomed. Eng.*, vol. 41, no. 4/5, pp. 365–391, 2013.

[10] Y. Zhou, H. Ren, M. Q.-H. Meng, Z. T. H. Tse, and H. Yu, "Robotics in natural orifice transluminal endoscopic surgery," *J. Mech. Med. Biol.*, vol. 13, no. 02, p. 1350044, 2013.

[11] S. Liu, D. Sun, and C. Zhu, "Coordinated motion planning for multiple mobile robots along designed paths with formation requirement," *IEEE/ASME Trans. Mechatronics*, vol. 16, no. 6, pp. 1021–1031, Dec. 2011.

[12] S. Kloder and S. Hutchinson, "Path planning for permutation-invariant multirobot formations," *IEEE Trans. Robot.*, vol. 22, no. 4, pp. 650–665, Aug. 2006.

[13] T. A. Vidal-Calleja, C. Berger, J. Solà, and S. Lacroix, "Large scale multiple robot visual mapping with heterogeneous landmarks in semi-structured terrain," *Robot. Auton. Syst.*, vol. 59, no. 9, pp. 654–674, 2011.

[14] Z. Wang and D. Gu, "Cooperative target tracking control of multiple robots," *IEEE Trans. Indust. Electron.*, vol. 59, no. 8, pp. 3232–3240, Aug. 2012.

[15] Y. C. Shiu and S. Ahmad, "Calibration of wrist-mounted robotic sensors by solving homogeneous transform equations of the form $AX = XB$," *IEEE Trans. Robot. Autom.*, vol. 5, no. 1, pp. 16–29, Feb. 1989.

[16] R. Y. Tsai and R. K. Lenz, "A new technique for fully autonomous and efficient 3d robotics hand/eye calibration," *IEEE Trans. Robot. Autom.*, vol. 5, no. 3, pp. 345–358, Jun. 1989.

[17] R. Horaud and F. Dornaika, "Hand-eye calibration," *Int. J. Robot. Res.*, vol. 14, no. 3, pp. 195–210, 1995.

[18] K. Daniilidis, "Hand-eye calibration using dual quaternions," *Int. J. Robot. Res.*, vol. 18, no. 3, pp. 286–298, 1999.

[19] F. C. Park and B. J. Martin, "Robot sensor calibration: Solving $AX = XB$ on the Euclidean group," *IEEE Trans. Robot. Autom.*, vol. 10, no. 5, pp. 717–721, Oct. 1994.

[20] K. H. Strobl and G. Hirzinger, "Optimal hand-eye calibration," in *Proc. 2006 IEEE/RSJ Int. Conf. Robots Syst.*, 2006, pp. 4647–4653.

[21] I. Fassi and G. Legnani, "Hand to sensor calibration: A geometrical interpretation of the matrix equation $AX = XB$," *J. Robot. Syst.*, vol. 22, no. 9, pp. 497–506, 2005.

[22] A. Malti and J. P. Barreto, "Robust hand-eye calibration for computer aided medical endoscopy," in *Proc. IEEE Int. Conf. Robot. Autom.*, 2010, pp. 5543–5549.

[23] Z. Zhao, "Hand-eye calibration using convex optimization," in *Proc. IEEE Int. Conf. Robot. Autom.*, 2011, pp. 2947–2952.

[24] M. K. Ackerman, A. Cheng, B. Shiffman, E. Boctor, and G. Chirikjian, "Sensor calibration with unknown correspondence: Solving AX= XB using Euclidean-group invariants," in *Proc. IEEE/RSJ Int. Conf. Intell. Robot. Syst.*, 2013, pp. 1308–1313.

[25] H. Zhuang, Z. S. Roth, and R. Sudhakar, "Simultaneous robot/world and tool/flange calibration by solving homogeneous transformation equations of the form $AX = YB$," *IEEE Trans. Robot. Autom.*, vol. 10, no. 4, pp. 549–554, Aug. 1994.

[26] F. Dornaika and R. Horaud, "Simultaneous robot-world and hand-eye calibration," *IEEE Trans. Robot. Autom.*, vol. 14, no. 4, pp. 617–622, Aug. 1998.

[27] L. Wu and H. Ren, "Finding the kinematic base frame of a robot by hand-eye calibration using 3D position data," *IEEE Trans. Autom. Sci. Eng.*, 2015, doi:10.1109/TASE.2016.2517674.

[28] A. Li, L. Wang, and D. Wu, "Simultaneous robot-world and hand-eye calibration using dual-quaternions and kronecker product," *Int. J. Phys. Sci.*, vol. 5, no. 10, pp. 1530–1536, 2010.

[29] H. Ren and P. Kazanides, "A paired-orientation alignment problem in a hybrid tracking system for computer assisted surgery," *J. Intell. Robot. Syst.*, vol. 63, no. 2, pp. 151–161, 2011.

[30] F. Ernst, L. Richter, L. Matthäus, V. Martens, R. Bruder, A. Schlaefer, and A. Schweikard, "Non-orthogonal tool/flange and robot/world calibration," *Int. J. Med. Robot. Comput. Assisted Surg.*, vol. 8, no. 4, pp. 407–420, 2012.

[31] N. Trawny, X. S. Zhou, K. Zhou, and S. I. Roumeliotis, "Interrobot transformations in 3-D," *IEEE Trans. Robot.*, vol. 26, no. 2, pp. 226–243, Apr. 2010.

[32] X. S. Zhou and S. I. Roumeliotis, "Determining 3-D relative transformations for any combination of range and bearing measurements," *IEEE Trans. Robot.*, vol. 29, no. 2, pp. 458–474, Apr. 2013.

[33] J. Wang, L. Wu, M. Q.-H. Meng, and H. Ren, "Towards simultaneous coordinate calibrations for cooperative multiple robots," in *Proc. IEEE/RSJ Int. Conf. Intell. Robots Syst.*, 2014, pp. 410–415.

[34] X. Yang, L. Wu, J. Li, and K. Chen, "A minimal kinematic model for serial robot calibration using POE formula," *Robot. Comput.-Integr. Manuf.*, vol. 30, no. 3, pp. 326–334, 2014.

[35] L. Wu, X. Yang, K. Chen, and H. Ren, "A minimal POE-based model for robotic kinematic calibration with only position measurements," *IEEE Trans. Autom. Sci. Eng.*, vol. 12, no. 2, pp. 758–763, Apr. 2015.

[36] M. Reed and B. Simon, *Methods of Modern Mathematical Physics IV: Analysis of Operators*. London, U.K.: Academic, 1978.

[37] J. Selig, *Geometric Fundamentals of Robotics*. New York, NY, USA: Springer, 2005.

[38] P. Corke, "Robot arm kinematics," in *Robotics, Vision and Control*. New York, NY, USA: Springer, 2011, pp. 137–170.

[39] H. Zhuang and Y. C. Shiu, "A noise-tolerant algorithm for robotic hand-eye calibration with or without sensor orientation measurement," *IEEE Trans. Syst. Man Cybern.*, vol. 23, no. 4, pp. 1168–1175, Jul./Aug. 1993.

[40] M. Zuliani, *Ransac for Dummies*. Santa Barbara, CA, USA: Vision Res. Lab., Univ. California, Santa Barbara, 2009.

[41] B. Triggs, P. F. McLauchlan, R. I. Hartley, and A. W. Fitzgibbon, "Bundle adjustment—A modern synthesis," in *Vision Algorithms: Theory and Practice*. New York, NY, USA: Springer, 2000, pp. 298–372.

Liao Wu received the B.S. and Ph.D. degrees in mechanical engineering from Tsinghua University, Beijing, China, in 2008 and 2013, respectively.

From 2013 to 2015, he was a Research Fellow with the Department of Biomedical Engineering, National University of Singapore. Since 2016, he has been a Vice-Chancellor's Research Fellow with the Australian Centre for Robotic Vision, Queensland University of Technology, Brisbane, QLD, Australia. His research mainly focuses on industrial robotics and medical robotics. His research interests also include fundamental theories, such as kinematics, calibration, and application of Lie group theory in robotics. He is also interested in engineering techniques for the development of mechatronic systems.
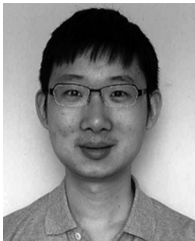
Jiaole Wang (S'14) received the B.E. degree in mechanical engineering from Beijing Information Science and Technology University, Beijing, China, in 2007 and the M.E. degree in human and artificial intelligent systems from University of Fukui, Fukui, Japan, in 2010. He is currently working toward the Ph.D. degree with the Department of Electronic Engineering, The Chinese University of Hong Kong, Shatin, Hong Kong.

His research interests include the areas of biomedical engineering, medical, and surgical robotics.

Lin Qi (M'08) received the B.S. and M.S. degrees in biomedical engineering from the School of Medicine, Tsinghua University, Beijing, China, in 2003 and 2006, respectively, and the Ph.D. degree from the Department of Electronic Engineering, The Chinese University of Hong Kong, Hong Kong, in 2013.

He is currently an Associate Professor with the Sino-Dutch Biomedical and Information Engineering School, Northeastern University, Shenyang, China. His research interests include medical robots and signal processing.

Keyu Wu (S'15) received the B.S. degree in bioengineering from National University of Singapore, Singapore, in 2013, where she is currently working toward the Ph.D. degree with the Department of Biomedical Engineering.

Her research interests mainly include visual servoing and motion planning for flexible surgical robots and statistical atlas construction for implant and robot design.

Hongliang Ren (M'06) received the Ph.D. degree in electronic engineering (specialized in biomedical engineering) from The Chinese University of Hong Kong, Hong Kong, in 2008.

He is currently an Assistant Professor and leading a research group on medical mechatronics with the Biomedical Engineering Department, National University of Singapore (NUS), Singapore. He is an affiliated Principal Investigator for Singapore Institute of Neurotechnology (SINAPSE) and NUS Advanced Robotics Center. From 2008 to 2010, he worked as a Research Fellow with the Laboratory for Computational Sensing and Robotics and the Engineering Center for Computer-Integrated Surgical Systems and Technology, Department of Biomedical Engineering and Department of Computer Science, The Johns Hopkins University, Baltimore, MD, USA. In 2010, he joined the Pediatric Cardiac Biorobotics Laboratory, Department of Cardiovascular Surgery, Boston Children's Hospital and Harvard Medical School, Boston, MA, USA, for investigating the beating heart robotic surgery system. Prior to joining NUS, in 2012, he also worked on a collaborative computer-integrated surgery project with the Surgical Innovation Institute, Children's National Medical Center, Washington, DC, USA. His main research interests include biomedical mechatronics, computer-integrated surgery, and robotics in medicine.

Max Q.-H. Meng (F'08) received the Ph.D. degree in electrical and computer engineering from University of Victoria, Victoria, BC, Canada, in 1992.

He has been a Professor of electronic engineering with Chinese University of Hong Kong since 2002, after working for ten years with the Department of Electrical and Computer Engineering, University of Alberta, Edmonton, AB, Canada, as the Director of the Advanced Robotics and Teleoperation Laboratory and holding the positions of an Assistant Professor (1994), Associate Professor (1998), and Professor (2000). He holds honorary positions as a Distinguished Professor with State Key Laboratory of Robotics and Systems, Harbin Institute of Technology, Harbin, China; a distinguished Provincial Professor with Henan University of Science and Technology, Luoyang, China; and the Honorary Dean of the School of Control Science and Engineering, Shandong University, Jinan, China. His research interests include robotics, perception and sensing, human–robot interaction, active medical devices, biosensors and sensor networks, and adaptive and intelligent systems. He has published more than 500 journal and conference papers and served on many editorial boards.

Dr. Meng is serving as an Elected Member of the Administrative Committee of the IEEE Robotics and Automation Society. He received the IEEE Third Millennium Medal Award.